RAMAN SPECTROSCOPIC STUDIES OF EQUINE LIVER ALCOHOL DEHYDROGENASE, ITS COENZYMES AND SUBSTRATES

BY

CHARLOTTE LEVIAN MARTIN

A dissertation submitted to the Graduate Faculty in Biochemistry in partial fulfillment of the requirements for the degree of Doctor of Philosophy, The City University of New York.

1987

This manuscript has been read and accepted for the Graduate Faculty in Biochemistry in satisfaction of the dissertation requirement for the degree of Doctor of Philosophy.

July 27, 1987
Date

Chair of Examining Committee

July 30, 1987
Date

Executive Officer

Supervisory Committee

The City University of New York

ABSTRACT

Raman Spectroscopic Studies of Equine Liver Alcohol Dehydrogenase, its Coenzymes and Substrate

by

Charlotte L. Martin

Adviser: Dr. Robert H. Callender
Co-Adviser: Dr. Donald L. Sloan

The solution Raman spectrum of equine liver alcohol dehydrogenase (EC-1.1.1.1., LADH) has been obtained. Its secondary structure as determined by a close examination of the Raman bands is somewhat different from its crystalline structure, as determined by X-ray diffraction.

The binary complex of the coenzyme, reduced nicotinamide adenine dinucleotide (NADH) and LADH has been studied. Using difference Raman spectroscopy, the Raman features of NADH bound to LADH have been determined. There are significant changes in the bound NADH spectrum relative to its solution spectrum. The data suggests that both the nicotinamide and the adenine moieties of NADH are involved in binding and at least one of the two NH_2 moieties is involved as well.

In order to understand the spectroscopy and to fully interpret the data in molecular terms as they relate to the organic mechanism occurring at the active site of the enzyme, LADH, Raman spectroscopy of reduced nicotinamide adenine

dinucleotide, NADH, and oxidized nicotinamide adenine dinucleotide, NAD^+, has been systematically carried out through the study of various fragments and analogues of these molecules. The effects of deuteration and pH on the exchangeable protons of NADH and NAD^+ also have been studied. By comparing the relative intensities and positions of the peaks in the Raman spectra of NADH and NAD^+ with those of their fragments and analogues, it has been found useful to consider these rather complicated molecules (NADH and NAD^+) as consisting primarily of the various components: adenine, two riboses, two phosphates and nicotinamide for the purpose of assigning their Raman bands.

The aromatic aldehyde ρ-(dimethylamino) benzaldehyde (DABA) a relatively poor substrate of LADH has been studied in an attempt at understanding the molecular details of this bound substrate and how it and other substrates bind at the active site of LADH. This compound when complexed to Zn^{2+} in diethyl ether has been used previously as a model for the enzyme substrate complex between LADH and DABA (46,47). Therefore, as a model of the substrate in the molecular environment of the enzyme active site the pre-resonance Raman spectra of the native DABA when ligated with zinc ion in methylene chloride and diethyl ether has been obtained. In addition, various isotopically labelled compounds of DABA (^{13}C, ^{2}H) have been studied in order to interpret the Raman spectra of DABA and the DABA-Zn^{++} models. We find that the DABA-Zn^{++} complexes in solution are excellent models for events which may occur <u>in situ</u>

with DABA, for their Raman spectra are essentially the same.

ACKNOWLEDGEMENTS

No piece of work, no matter how small, is ever done in isolation. I would like to express my deepest appreciation to my mentors, Dr. Robert H. Callender and Dr. Donald L. Sloan for the support, guidance and encouragement they provided throughout this research. Without these I would not have been involved in this work.

For my mother

Luna Viola Cooper

TABLE OF CONTENTS

List of Tables

Page #

Figure Legends

INTRODUCTION

Liver alcohol dehydrogenase, LADH (E.C. 1.1.1.1), is one of several alcohol dehydrogenases which utilize the coenzyme nicotinamide adenine dinucleotide (NAD^+) and its reduced form NADH in its oxidation-reduction reactions. These coenzymes are well known for their ubiquity throughout most organisms. In relation to most dehydrogenase-catalyzed redox reactions, the oxidized form (NAD^+), acts as an oxidant by accepting a hydride onto the C4 position of the pyridine ring while the reduced form (NADH) behaves as a reductant by contributing a hydride from this position (equation 1).

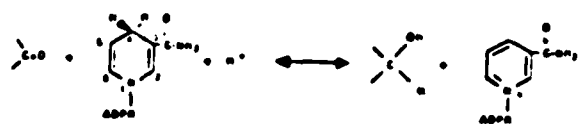

(equation 1)

The means through which this reaction is carried out at the active site of the enzyme has received considerable attention over the years. Of importance is the question of how coenzymes and substrates bind at the enzyme's active site. It is well known that the kinetic mechanism of liver alcohol dehydrogenase is the sequential Theorell-Chance mechanism. That is to say, during catalysis it is observed that the coenzyme binds before the

substrate binds. The product leaves, then the reduced or oxidized coenzyme leaves depending on the direction of the equation (equation 2).

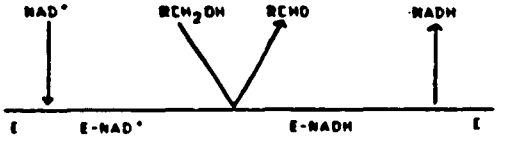

(equation 2)

In this reaction scheme there are several intermediates. There is the formation of the binary complex in which the coenzyme binds to the enzyme, and the formation of the ternary complex in which the substrate binds to the binary complex (Figure 1). The binary complexes $ENAD^+$ and ENADH, where E represents the ADH enzyme, are known to be quite stable (7,14,42,44,69). Nevertheless, the organic mechanism via which substrate is converted to product is not understood. Notwithstanding, however, some information on these types of interaction has become available through X-ray crystallographic studies on various dehydrogenases (7,14,42,44,69).

These X-ray studies show that there are sizable conformational changes in the enzyme when the coenzyme binds to the enzyme. In these studies, electron-density differences are calculated to give the location of the ligand within the enzyme. However, the nature of the interaction(s) between the ligand and protein are only deduced and not studied directly. From other studies it has been shown that the adenine moiety is essential for the binding of NADH to the enzyme (43,88). In one such study,

Figure 1: The general reaction scheme of LADH; the oxidation and reduction of nicotinamide adenine dinucleotide and substrates; the formation of binary (LADH/NADH; LADH/NAD^+) and ternary (LADH/NADH/aldehyde, LADH/NAD^+/alcohol) complexes of enzyme/coenzymes and enzyme/coenzymes/substrates.

Nicotinamide Adenine Dinucleotide ----> NADH & NAD^+

Liver Alcohol Dehydrogenase ----> LADH

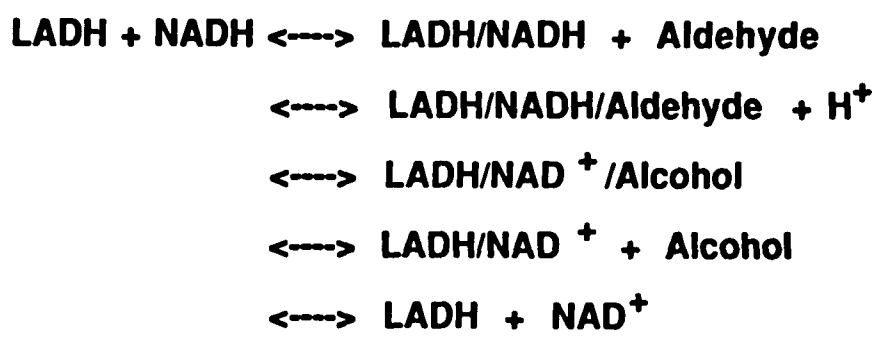

Figure 1.

Hollis (43) supports the role of the adenine moiety and further suggests the involvement of the nicotinamide moiety in binding.

Using Raman spectroscopy, in our laboratory, in an attempt at understanding the enzyme's mechanism, the approach has been to understand the Raman spectra of LADH, the LADH/NADH binary complex and the LADH/NADH/DABA ternary complex. Raman spectroscopy has come into prominence as a tool for studying macromolecules and biological systems in the last few years. Specifically, the studies of several biologically significant chromophore containing systems have been possible. These studies encompass work on enzymatic systems (18,20), visual pigments and bacteriorhodopsin (17,58,98), and hemoproteins (39,85). From these studies it seems possible that this technique may offer significant promise in the field of protein chemistry i.e. protein conformational analysis, interaction of macro and micro molecules with proteins, DNA-protein complexes, enzyme-coenzyme and substrate complexes, DNA research and research on a panoply of cytosolic components. In our studies this technique has proven useful in elucidating the secondary structure of LADH in solution, providing insight into how NADH binds to LADH and the binding of ρ-dimethylamino benzaldehyde (DABA), an aromatic substrate, to the enzyme.

One of the important features of Raman scattering is the frequency shift of the scattered light relative to that of the incident light by amounts relating to the molecule's normal mode frequencies. Hence, Raman spectra give detailed information on the

vibrational motions of atoms in molecules. With this in mind, the technique has been employed to further our understanding of the secondary structure of LADH in solution. We have observed, from these studies, upon examination of the Raman bands, that the secondary structure of the enzyme compared to that determined by X-ray diffraction is slightly different.

Difference spectroscopy, the result of subtracting the Raman spectrum of LADH from that of the LADH/NADH binary complex, was obtained from an interleaving fashion of $A_1B_1B_2A_2A_3...B_nA_n$, where A_X represents the Raman spectrum of the binary complex taken at time X, and B_X the Raman spectrum of the enzyme taken at some other time X during the experimental process. The sum of A spectra minus the sum of B spectra shows that there are significant changes in the spectrum of bound NADH as compared to that in solution. It is also apparent that at least one of the two NH_2 moieties of NADH is involved in binding and the nicotinamide and adenine moieties, are significantly involved when NADH binds LADH.

In order to investigate the significance of the Raman spectra of NADH/NAD^+ in solution and when bound to the enzyme, LADH, we obtained the Raman spectra of various fragments and analogues of NAD^+ and NADH. In particular we report the Raman spectra of adenine, adenosine, AMP, ADP, ADPR, NMN^+, NMNH, 1-methylnicotinamide iodide, 9-ethyladenine, and 3-$PAAD^+$. The effects of pH and the deuteration of the exchangable protons on the Raman spectra of NADH, NAD^+ and their fragments and analogues

have been studied as well. From these studies the peaks in the NAD^+ and NADH spectra can be assigned to individual groups on these coenzymes.

A more complete examination of the Raman features of NAD^+ and NADH come from these studies, for other studies (8,41,65,72) have been concerned mostly with the assignment of the C=O stretching mode with little or no discussion of the other spectral features. Several other more recent ultraviolet resonance Raman studies of NADH and its analogues (12,66,72) delve more into the understanding of the spectral features of NADH, and have presented a more thorough examination of some of these spectral characteristics. Studies on molecules containing portions of NADH and NAD^+ have been carried out as well (51,53,75). Our results are similar to the data of these studies. In addition we have studied the assignment of particular bands in terms of specific nuclear motions where these previous studies have made such an assignment.

As an initial approach to understanding the molecular properties of the aromatic aldehyde p-dimethylamino benzaldehyde (DABA) in solution and in the molecular microenvironment of the substrate site of LADH, resonance Raman spectroscopy has been employed in this work. In resonance Raman spectroscopy, the incident light wavelength coincides with an absorption center on the molecule. This results in the enhancement of the Raman cross-sections for normal modes associated with this center. As this is the case, only Raman scattering resulting from the absorption

center is observed. Therefore, it is possible to analyze these patterns and deduce the overall structure of the absorption center. If the wavelength of the incident light is in pre-resonance with the absorption center, that is to say, if the wavelength is relatively close to the absorption center, then the Raman cross section of the absorption center modes are relatively enhanced over those of the other regions of the molecule by several orders of magnitude.

In its UV/Vis spectrum, DABA has an absorption band at 352 nm whereas NAD^+/NADH and LADH have absorption bands at 260 nm and 280 nm respectively. In our laboratory these properties were exploited to obtain Raman spectrum of the LADH/NADH/DABA ternary complex, whose features are primarily those of DABA. As an approach to understanding the Raman spectrum of bound DABA, a series of pre-resonance Raman data was collected for DABA, isotopically labelled DABA {namely DABA deuterated at the aldehydic proton (CDO), ^{13}C labelled at the carbonyl carbon (^{13}CHO), ^{13}C and ^{2}H labelled at the functional group (^{13}CDO), and deuteration of the 3 and 5 ring protons (2D)} and Zn^{++} complexes, of native DABA as well as its isotopic derivatives. In contrasting the enzyme bound DABA data to those of the $zinc^{++}$-DABA complexes in solution it seems that the $zinc^{++}$-DABA complex is a suitable model for the aromatic substrate DABA at the active site of LADH.

DISCUSSION OF ALCOHOL DEHYDROGENASE

Alcohol dehydrogenase's activity has been observed in numerous animal and plant tissues as well as in some microorganisms. A few examples are the human liver, horse liver, rat liver (90), frog and cattle retina (97), yeast, mouse serum, erythrocytes of some lower vertebrates, peas, corn, rice, parsley (90), sugar beets, spinach, sun flower and tobacco (5), Asperigillus niger, Escherichia coli (90), Neurospora crassa (63,64) and a few more.

The primary studies of ADH began at the end of the 19th century when it was observed that various animal tissues oxidized alcohols (90). As described by Sund and Theorell, Buchner and Gaunt coined the term "alkoholoxydase" for the alcohol oxidizing enzyme in acetic acid bacteria (90). Batelli and Stern studied the properties of ADH in various animal tissues in 1909. It was then that acetone-dried preparations and cell-free ADH solutions were first used. The first experiment with the soluble yeast enzyme was not performed until 1933 (90). During that time it was implied that NAD^+ functioned as a coenzyme in the oxidation-reduction reaction (eq. 1). It was not until 1936, that von Euler and his co-workers established that NAD^+ was indeed the coenzyme (90). In 1937 Negelein and Wulff sucessfully crystallized the yeast enzyme, (90) and in 1948 Bonnichsen and Wassen (90) isolated ADH from horse liver in crystalline form.

ADH catalyses many reactions. It is well known that ADH does not have a unique specificity for substrates as its reacts with a variety of normal and branched-chain aliphatic and aromatic alcohols, both primary and secondary, various carbonyl compounds and a series of analogs of NAD^+/NADH (90). Examples are ADH's involvement in the degradation of fructose, the reduction of glyceraldehyde to glycerol, and the reduction of retinal (the aldehydic chromophore of visual pigments) to the corresponding alcohol, retinol.

Electrophoretic studies of equine liver alcohol dehydrogenase (LADH) (E. C. 1.1.1.1.) indicate that LADH contains two components, a main component and a minor component. These components, it has been shown, show somewhat different specificities. Consequently, three main isozymes are formed by the dimeric combination of these two different components. These components, are not active in the monomeric state. However, in the dimeric forms they are active and subsequently show various specificities. Accordingly, these components have been named. The steroid active component has been named S while the ethanol active component is called E (14). The major isozymes are therefore EE, ES, and SS. Although their names may suggest substrate specificity it is important to note that EE and SS both have steriod and ethanol activity respectively, albeit with low reaction rates.

It is worth mentioning that there are six amino acid differences between the primary structures of E and S.

Apparently, the two proteins are synthesized from different autosomal gene loci, and post transcriptional modification of the three forms of the protein lead to various subfractions. Namely, EE', EE'', EE''' where the prime represents a decrease in cathodic electrophoretic mobility.

The main isozyme of the commercial preparation of equine liver alcohol dehydrogenase is EE. Its molecular weight is 80,000 MW (56), with an extinction coefficient of 3.57 X 10^5 M^{-1} cm^{-1} at 280 nm. This isozyme contains 374 amino acid residues of which 14 are cysteines. It is well known that the native enzyme contains two Zn(II) ions per monomer, one of which participates in catalysis (96) while the other is found in a structural site. It is believed that this structural site's zinc ion is primarily for the stabilization of the quaternary structure of the enzyme (33).

The catalytically essential zinc ions, differs in physiochemical properties from those of the structural zinc ion. It has been shown by $^{65}Zn^{2+}$ exchange that the structural zinc ion can be differentiated from the catalytic zinc ion, and that these zinc ions can be differentially labelled as well (34). X-ray studies suggest that the catalytic zinc ion is coordinated in a distorted tetrahedron by two sulfur atoms from cys-46 and cys-174, one nitrogen atom from his-67, and one oxygen from a water molecule which is believed to be replaced by the oxygen of the substrate during catalysis (Figure 2). The non-catalytic zinc ion, on the other hand, has been measured as being 2.06 nm away from

Figure 2: A schematic representation of the active site of equine liver alcohol dehydrogenase, depicting the coenzyme and substrate binding domains and the coordination of the active site zinc to sulfur of Cys-174, Cys-46 and nitrogen of His-67, and the oxygen of water.

Figure 2.

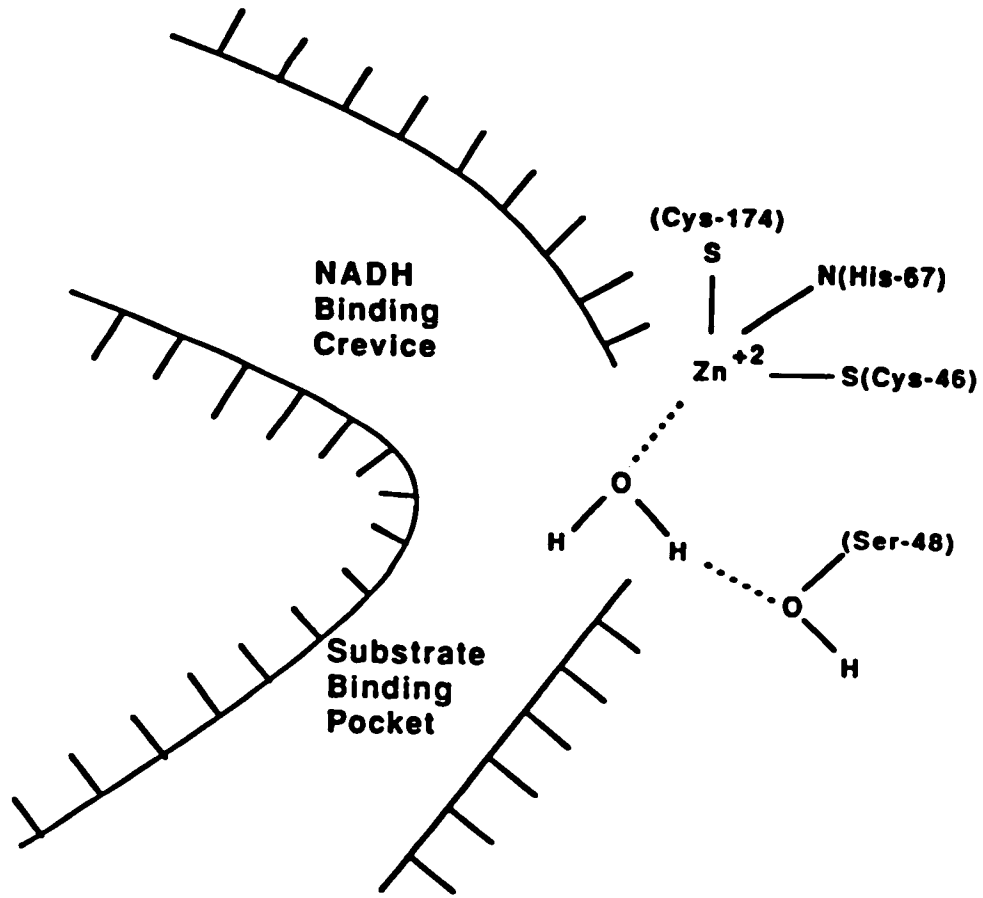

Sketch of the Active Site of Horse Liver Alcohol Dehydrogenase

the catalytic site and is coordinated in a distorted tetrahedron by four sulfur atoms from cys-97, cys-100, cys-103 and cys-111 (14). Furthermore, it has been noted that both catalytic and non-catalytic zinc ions play a substantial structural role in the enzyme (56).

Eklund et al. (37) have shown via the crystal structure that LADH has a specific coenzyme binding site near the catalytic site (Figure. 2). At this site, the adenine moiety of NAD^+/NADH lies on a β-pleated sheet region while the ribose and pyrophosphate groups fold in such a way as to accommodate the nicotinamide moiety in making van der Waals contact with the catalytic zinc ion. The coenzyme upon binding induces a significant protein conformational change, enhancing the substrate binding to the hydrophobic active site of the enzyme. Evidence along these lines come from optical and electron paramagnetic resonance spectroscopic (EPR) studies, which show that the 296 K optical spectrum of Cu (II)·LADH shows a small red shift upon NADH binding with an unchange molar extinction coefficient. In terms of EPR, the hyperfine splitting of Cu (II)·LADH, it was observed, went unchanged upon NADH binding. Although no observed changes in the zinc (II) ligand takes place, it is mentioned that perhaps changes in protein conformation do cause small pertubations at the metal center. It is becoming apparent that the catalytic zinc ion in liver alcohol dehydrogenase has a multifunctional role as well.

It has been proposed by some researchers that during catalysis the active site metal ion activates the substrate via a direct coordination between the metal and substrate, thereby operating as a Lewis acid. The experimental evidence along this line shows that, when the zinc ion has been replaced by cobalt ion in LADH, the binding of anions, such as azide, acetate or hydrogen sulfide causes characteristic changes in the spectra of the catalytic cobalt ion in free cobalt (II)-LADH, namely the disappearance of the 520 nm absorption band with the concomitant appearance of a band around 575 nm (56). Similarly in ternary complexes such as Co^{++}-LADH/NAD^{+}/acetate or 2,2,2-trifluoroethanol (56) spectral changes upon anion binding have been observed.

On the other hand while a variety of information regarding direct coordination of the zinc metal ion to substrate and/or coenzyme has been presented, the mechanistic role of zinc ion in LADH is still a subject of active investigation and discussion. Fluorimetric studies by Iweibo and Weiner (45) showed that substrate competitive inhibitors form ternary complexes with the metal free enzyme and NADH. In addition Young and Wang (106) have shown no spectroscopic changes which are characteristic of coordination of azide to the catalytic ion of the native and cobalt (II) zinc (II) mosaic enzyme. Furthermore, kinetic studies and binding studies have argued against such coordination. Sloan et al. (84) using nuclear magnetic resonance spectroscopy, studied the substrate interaction with Co^{++}-LADH. They argue that the

paramagnetic effects of Co (II), at the catalytic site, on the relaxation rates of the methyl protons of isobutyramide (IBA) at 100 and 200 MHz indicate that IBA binds at a site 9.1 Å from the catalytic Co (II). This distance, they observed, decreased to 6.9 Å upon NADH binding. Also they determined a Co (II) to methyne proton distance of 6.6 Å, indicating that a conformational change may lead to the formation of a second sphere enzyme Co (II) IBA complex in which a hydroxyl or water ligand intervenes between the metal and the IBA. With the substrate, ethanol, they showed that upon ethanol binding, the paramagnetic effects of Co (II), at the active site, on the relaxation rates of the ethanol protons at 100 and 220 MHz showed that ethanol binds at a distance of 12-14 Å from the Co (II). In the abortive complex, LADH/NADH/ethanol it was shown that the ethanol binds at a distance of 6.3 Å. Hence they have postulated that a possible role of the catalytic cobalt ion may be the activation of a hydroxyl or water ligand which, it is thought, polarizes the aldehyde carbonyl group by hydrogen bonding. Moreover, it has been suggested that the metal ion influences the dynamics of coenzymes and their analogs binding, although molecular evidence for direct binding of coenzymes/analogs to the metal ion is not available.

In spite of all of the suggestions as to how the zinc ion might be involved in LADH's catalysis, much more information is needed for the proper understanding of the molecular details of the catalytic cycle. In particular, that which might lock

everything in place in terms of the mechanism is the number and chemical nature of all the intermediates formed during the ternary complex interconversions. A problem of concern with these types of studies is the formation of stable ternary complexes. Preliminary information has recently become available through studies of the very poor LADH substrate ρ-dimethylamino benzaldehyde (DABA). DABA forms a very stable ternary complex with LADH/NADH, hence an LADH/NADH/DABA complex is formed. DABA has a strong absorption band at 352 nm (ε=3.0 X 10^4 M^{-1} cm^{-1}) in solution. Angelis et al. (6) have shown that DABA is converted to the corresponding alcohol in the presence of NADH and LADH around pH 7.0. However at pH 9.6 DABA forms a very stable ternary complex with a shift of λmax to 380 nm (ε=2.9 X 10^4 M^{-1} cm^{-1}). Peticolas et al. (47) have reported the Raman spectra of DABA dissolved in water buffer and other solvents and the spectrum of the stable ternary complex LADH/NADH/DABA. They reported major changes in the Raman spectrum of DABA when bound to the enzyme complex, compared to that in solution. In these studies the tentative assignment of the Zn^{++}-O bond was determined as being 394 cm^{-1} in the LADH/NADH/DABA ternary complex. In this work other Raman studies were done in which the carbonyl oxygen was isotopically labelled (^{18}O) and the ternary chemical intermediate and the Lewis acid complex formed. There was no obvious confirmation of the Zn^{++}-O bond since the isotopically labelled carbonyl oxygen of DABA did not give the anticipated changes in the

Zn^{++}-O band. That is to say, no significant shift of the "assigned" Raman band for the Zn^{++}-O was observed under these conditions.

Structural studies of LADH has been underway by several investigators. Eklund and his co-workers (35) reported the three dimensional structure of crystalline LADH at 2.4 Å resolution with an X-ray diffraction analysis. They showed that the enzyme contains 29% α helix, 34% β-pleated sheet and 37% random coil under these conditions. Williams and his group (101), using Raman spectroscopy, calculated (based on the amide I bands) that LADH contained a relative low percentage of α helix (18%). Our studies have confirmed the latter results.

RAMAN EFFECT

Raman spectroscopy is a means of acquiring information on the normal vibronic, torsional, and bending modes of a molecule. The Raman scattering effect comes from with the interaction of the incident light with the electrons in the illuminated molecule. It is known that when a sample is illuminated with a beam of light at frequency (ν) an oscillating dipole is induced in the molecule.

The classical expression of this effect is:

$$\mu_{ind} = \alpha(\nu) \cdot E(\nu)$$

where μ_{ind} is the induced dipole, α is the electric polarizability tensor of the molecule at frequency ν, and E is the electric field vector of the light. If the time variation of the electric field of the light is defined as:

$$E(t) = E_0 \cos 2\pi\nu t$$

then:

$$\mu_{ind} = \alpha(\nu) \cdot E_0 \cos 2\pi\nu t.$$

We will assume for simplicity that the electric polarizability tensor of the molecule is treated as a number $\alpha(\nu)$ instead of the tensor quantity it is. Since the molecule is vibrating at some normal mode frequency, its polarizability will not be constant. When the molecule moves the electrons react and at each nuclear position a change in polarizability takes place. This phenomenon can be defined as:

$$\alpha(\nu) = \alpha_0(\nu) + \alpha'(\nu) \cos 2\pi\nu' t$$

where α_0 is the polarizability of the molecule at its equilibrium nuclear configuration, $\alpha'(\nu)$ is the change in polarizability when there is nuclear motion and ν' is the vibrational frequency of this nuclear motion. Introducing this equation into the definition of the induced dipole, the equation which predicts what the induced dipole will be in the molecule is then:

$$\mu(t) = E_0[\alpha_0(\nu) + \alpha'(\nu)\cos 2\pi\nu' t]\cos 2\pi\nu t$$

$$= E_0\alpha_0(\nu)\cos 2\pi t\nu + E_0\alpha'(\nu)\cos 2\pi\nu' t\cos 2\pi\nu t$$

$$= \mu(t) + \mu'(t)$$

where $\mu(t)$ is the normal induced dipole oscillating at frequency (ν) which results in elastic light scattering, and $\mu'(t)$ gives rise to the Raman spectrum. From the geometric definition that $\cos A\cos B = 1/2[\cos(A + B) + \cos(A - B)]$ this effect can be demonstrated as:

$$\mu'(t) = 2\{E_0\alpha(\nu)[\cos 2\pi(\nu + \nu')t + \cos 2\pi(\nu - \nu')t]\}.$$

From this equation it is apparent that a dipole oscillating at a given frequency ν will emit radiation at frequencies $\nu + \nu'$ and $\nu - \nu'$. The position of the emission lines relative to the exciting frequency permits the measurement of the vibrational frequency ν' if ν is known and $\nu + \nu'$ or $\nu - \nu'$ is measured. The band at $\nu + \nu'$ is called the anti-Stokes band whereas that of $\nu - \nu'$ is called the Stokes band. While explaining this phenomenon, it is envisioned that the Raman effect is a two photon event. The complex takes up one photon of frequency ν and emits one at either $\nu + \nu'$ or $\nu - \nu'$.

When the incident radiation frequency lies at or near an absorption band, the Raman effect is enhanced. This enhancement is known as resonance or near resonance Raman spectroscopy. The resonance effect yields a large cross section enhancement of particular Raman bands.

For micromolecules the Raman effect compliments the infrared spectroscopy. Transitions which give rise to the Raman bands must have a polarizability which changes with nuclear motion, other than having a fixed dipole that changes. As this is the case, some transitions which are low in intensity in one technique may be high in the other. For highly asymmetric macromolecules, the Raman and the infrared effects give rise to essentially the same array of bands. The primary advantage of Raman spectroscopy is the fact that water has a relatively poor Raman spectrum, making the study of biological systems, which contain water, easy. Moreover, only small amounts of samples are needed i.e. enough sample to fill the volume of the laser beam. We have performed measurements of as little as 10 μl.

In comparison to other systems, for instance, nuclear magnetic resonance spectroscopy (NMR), NMR techniques require very high concentrations of the sample (although this has improved dramatically for protons in recent years) or an enrichment of a particular substance's magnetic nuclei in order for these resonances to be obtained. Furthermore, fourier transform experiments can be performed for days or weeks. X-ray

crystallography, while providing useful information on atomic positions, seldom gives specifications of electronic structure such as bonding properties. In addition it requires that the sample is in the crystalline state, which may not always mimic the in vivo situation. In addition, not all samples can be crystallized. Ultraviolet/visible absorption spectroscopy although useful in making provision for the understanding of the excited state structure of a molecule does not compare to Raman spectroscopy, which provides information not only of the excited state structure of a molecule, but the ground state as well.

Despite its success Raman spectroscopy is, however, not without its limitations. The Raman spectra can easily be obscured by flourescence, resulting often from impurities. In addition, for an adequate spectrum with a good signal to noise ratio the sample requires high concentrations, in the range of approximately 0.01-0.1 M or higher. These concentrations are much higher than those used in NMR experiments. Additionally, it is not always easy to interpret the Raman data. Current theories relating Raman bands to normal mode vibrations and these to structure are not yet routine for large molecules.

To date many of the Raman bands found in protein spectra have been assigned to specific peptides or side chain vibrations in proteins, particular phosphates or bases in nucleic acids and conformation and conformational changes (i.e. differences between α helices, β sheets, and random coils) in proteins. Moreover rich

information pertaining to secondary structures of proteins can be made available from the Raman bands of the amide I and amide II transitions. In addition, hypochromicity in Raman spectra can often lead to the understanding of various states in some molecules e.g. base stacking or hydrogen-bonding in polynucleotides.

A Raman spectrometer consists essentially of a light source e.g. a laser beam of monochromatic radiation, a sample compartment, a monochromator, a photomultiplier system or a photo diode array as a detector, and an electronic signal-processing unit (Figure. 3).

Figure 3: Schematic representation of Raman spectrometer; depicting its light source, sample compartment, monochromater, detector, and electronic signal-processing unit.

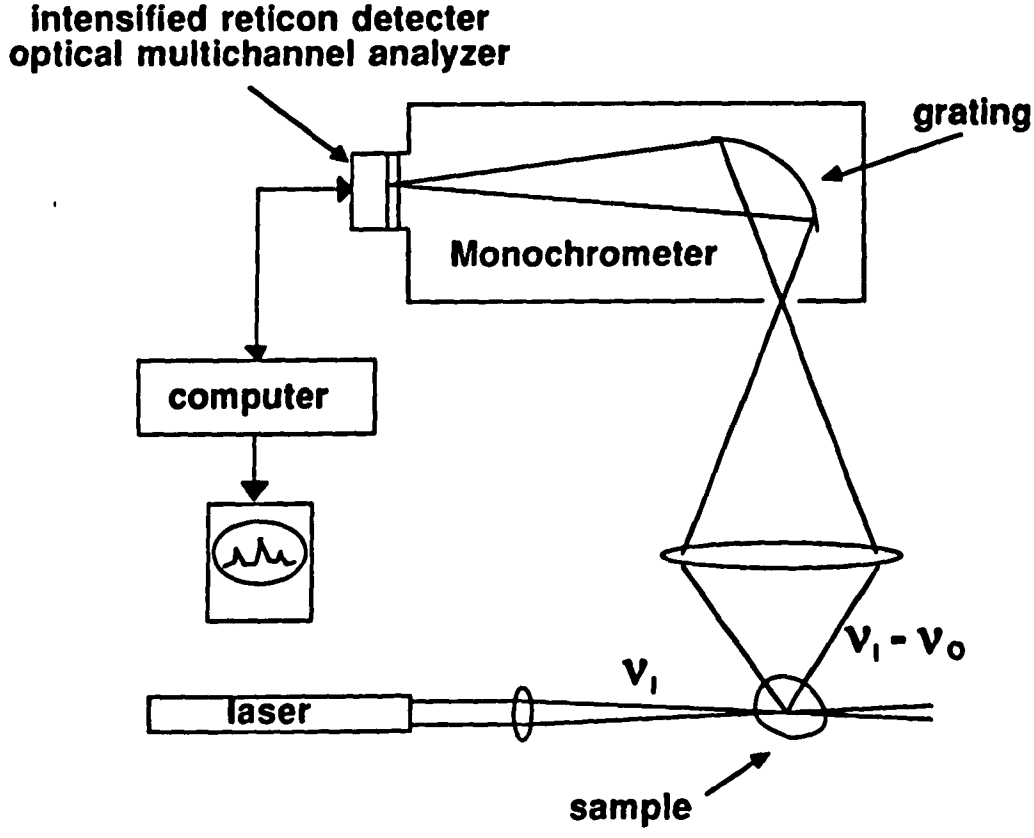
intensified reticon detecter
optical multichannel analyzer
grating
Monochrometer
computer
$\nu_l - \nu_o$
ν_l
laser
sample

Figure 3.

MATERIALS AND METHODS

MATERIALS. LADH was purchased from Boehringer Mannheim Co. (Indianapolis, IN). The collodion bag vacuum concentrator was supplied by A. H. Thomas (Philadelphia, PA). Collodion bags were obtained from Schleicher & Schuell (Keene, NH). The centricon 30 microconcentrator was purchased from AMICON (Danver, MA). NADH (Grade III), NAD^+ (Grade III), 3-$PAAD^+$, NMN^+, NMNH, 1-methylnicotinamide iodide, 9-ethyladenine, adenine (Sigma grade), adenosine (Sigma grade), ADP (grade I), AMP (Sigma grade), p-(dimethylamino) benzaldehyde (DABA), and adenosine 5'-diphosphoribose were purchased from Sigma Chemicals Co. (St. Louis, MO). $ZnCl_2$ was purchased from Mallinckrodt, Inc. (St. Louis, MO). Anhydrous diethyl ether was obtained from either J. T. Baker Chemical Co. (Phillipsburg, NJ) or Fisher Scientific Co. (Fair Lawn, NJ). Isotopically labelled DABAs were prepared by the laboratories of Dr. J. Lugtenburg (Gorlaeus Laboratories, State University Leiden, Leiden, Netherlands) and Dr. V. Balogh-Nair (The City College of New York, N. Y., N. Y. 10031).

ENZYME PREPARATION. Liver alcohol dehydrogenase which is purchased as crystals suspended in 20 mM potassium phosphate buffer pH 7.0; 10% ethanol was prepared by methods as described below.

The crystals of LADH, which had settled at the bottom of the shipping vial were gently suspended using a pasteur pipette. The suspension was then transferred to a centrifuge tube and centrifuged for 20 minutes at 4°C at 6000 x g. The supernatant was aspirated off and the pellet was suspended in 0.05 M pyrophosphate buffer, pH 9.60. The enzyme suspension was centrifuged for 10 minutes at 4°C at 6000 x g. The supernatant was then removed and exhaustively dialysed against 0.1 M pyrophosphate buffer, pH 9.60. It was then concentrated using a collodion bag vacuum concentrator.

ENZYME ASSAY. The enzymatic activity was determined by the method of Dalziel (28). In two cuvettes were added separately 250λ of 30 mM NAD^+, 2.6 ml 20 mM pyrophosphate pH 8.8 and 30λ 10% ethanol. To the reference cuvette 100λ of buffer was added. To the sample cuvette 100λ containing 7-12 μM LADH was added. The sample was monitored at 340 nm for $t_{0.2}$ (the time it takes for the optical density to reach 0.2). The temperature was maintained at 23°C. The concentration of the enzyme was determined spectroscopically using $\varepsilon_{280}=3.57\times10^{4}M^{-1}\ cm^{-1}$.

PREPARATION OF DEUTERATED LADH. The LADH enzyme was diluted with 0.1 M pyrophosphate buffer pD 9.60 (pD=pH+0.4), containing D_2O. The preparation was allowed to sit overnight according to the process of Blout et al. (10). It was then

concentrated by a centricon 30 microconcentrator.

PREPARATION OF THE BINARY COMPLEX OF LADH/NADH. The complex was formed by mixing a 1:2 molar ratio of LADH:NADH according to the method of DeTraglia *et al.* (32). Under these conditions the complex formation is almost 100% (32), with no excess of NADH or LADH. The complex formation was verified spectroscopically by the shift in NADH's λ_{max} from 340 nm to 325 nm.

PREPARATION OF NADH, NAD^+, THEIR FRAGMENTS AND ANALOGUES. The samples were dissolved in 0.1 M pyrophosphate buffer, pH 9.60, or phosphate buffer, pH 7.0, 5.0, 4.0, or 3.0 depending on the necessary experimental condition. Had the pH of the buffer changed because of the basicity or acidity of the coenzyme, fragment or analogue, it was adjusted to the appropriate pH for the given experiment by the addition of dilute phosphoric acid or dilute potassium hydroxide.

The concentration of NADH and NAD^+, their fragments and analogues were determined spectroscopically using known values of extinction coefficients or by the addition of determined volumes of buffer to preweighed vials of known quantities.

PREPARATION OF DABA-Zn^{++} COMPLEX. 38.8 mg DABA and 43.0 mg $ZnCl_2$ were dried *in vacuo* over phosphorus pentoxide. Both were

used immediately or stored over phosphorous pentoxide in vacuo until use. In the case of DABA, it was stored in the dark. Anhydrous diethyl ether or methylene chloride used in these preparations were determined to be dry enough upon arrival from the industrial houses. After being opened diethyl ether was dried with sodium. When in use, 400 ml of either anhydrous diethyl ether or methylene chloride was added to DABA. For a saturated solution of $ZnCl_2$, the $ZnCl_2$ was added to 100 ml of either solvent. A 1:1 (v/v) mixture, of both solutions, was prepared and considered the DABA-Zn^{++} complex by the criteria of the shift in λmax from 327 nm when free in solution to 372 nm or 380 nm when in complexation to zinc ion in either diethyl ether or methylene chloride. All nonaqueous solutions were prepared in an argon atmosphere.

SAMPLE HANDLING AND THE RAMAN MEASUREMENTS. All samples were placed in a fluorescence cuvette and where necessary, the cuvette was placed in a thermobath and thermostatted in relation to the experiment. For the solution spectra of the enzyme the bath was maintained at 8°C. For the experiments involving the binary complex of NADH/LADH and the reference sample of LADH in solution the temperature was maintained at 4°C.

Samples of NADH, NAD^+, their fragments and analogues were measured at ambient temperature with the exception of adenine and adenosine at pH values lower than 9.6. These samples, because of

their low solubilities under ambient conditions, were measured at 60°C. All DABA samples, with or without zinc (II), were measured at ambient temperature. The temperature for all samples was maintained by a thermal bath/circulator. Ultraviolet/visible spectral measurements were obtained before and after each Raman measurement. No obvious changes in the absorption spectra were observed, indicating that no appreciable degradation of samples occurred during the Raman measurement. The Raman spectra of all samples were obtained by one of these two systems: (1) a standard scanning system consisting of a Spex 1401 double spectrometer controlled by a Compudrive controller (CD2A, Spex Industries, Metuchen, NJ), a cooled RCA 31034 photomultiplier, and photon-counting electronics; (2) an OMA system which consists of a Triplemate Spectrometer (Spex Industries, Metuchen, NJ) and a solid state detector system-Model 1420 water-cooled photodiode array and Model 1218 controller (EG&G, Princeton Applied Research, Princeton, NJ). Both spectrometers were interfaced to a LSI-11 microcomputer (Digital Equipment Corp., Marlboro, MA), which was also used for data analysis. All spectral lines measured with the OMA system were calibrated against known lines of toluene. Spectra measured with the scanning spectrometer are accurate to within ±2 cm^{-1}. The OMA system has an accuracy of ±1.5 cm^{-1}. Most spectra were measured using either 488 nm or 514.5 nm lines from a model 165 argon ion laser (Spectra Physics, Mountainview, CA). Blue-green lines from a Coherent (Palo Alto, CA) Model CR-

2000 krypton ion laser were also used. The organic solvent buffer background Raman spectrum has been substracted from the presented data in all instances.

RESULTS AND DISCUSSION

Structural studies of LADH

Figure 4 shows a typical Raman spectrum of LADH at pH = 9.60. Most of the peaks can be attributed either to the protein backbone or to amino acid "R-groups". Assignments were made by comparisons with Raman spectra of other proteins and amino acids in solution (54,78). Table 1 lists the preliminary assignments of most peaks to various parts of the enzyme.

Aromatic residues are known to give strong Raman lines. LADH has only 2 tryptophan (Trp) and 4 tyrosine (Tyr) residues. Thus contribution from these amino acid groups is expected to be small. For example, the 850 cm^{-1} and 831 cm^{-1} bands commonly associated with tyrosine (83) are only barely visible. However, there are 18 phenylalanine (Phe) residues in LADH, and they are responsible for the prominent sharp peak at 1003 cm^{-1} and for other smaller bands. Peaks from aromatic amino acid residues are known to be insensitive to the conformational state of the protein (54).

There are two prominent bands due to the peptide backbone of the enzyme. The amide I band appears at 1668 cm^{-1} and the amide III bands are at 1230^{sh}, 1245, and 1265^{sh} cm^{-1}. Raman spectral analysis of the enzyme in D_2O shows that the amide III bands shift towards 900-1000 cm^{-1} as expected (Figure. 5). A small broad structure remains at 1200-1300 cm^{-1} which may be due to other parts of LADH or to incomplete proton/deuterium exchange. Both

Figure 4: Raman spectrum of liver alcohol dehydrogenase in 0.1 M pyrophosphate buffer pH 9.6. Sample was maintained at 8 °C. Laser line was 488.0 nm with incident power of 110 mW. Dispersive grating was 1200 cm^{-1} with slit width of 100 μM, giving a final resolution of 6 cm^{-1}.

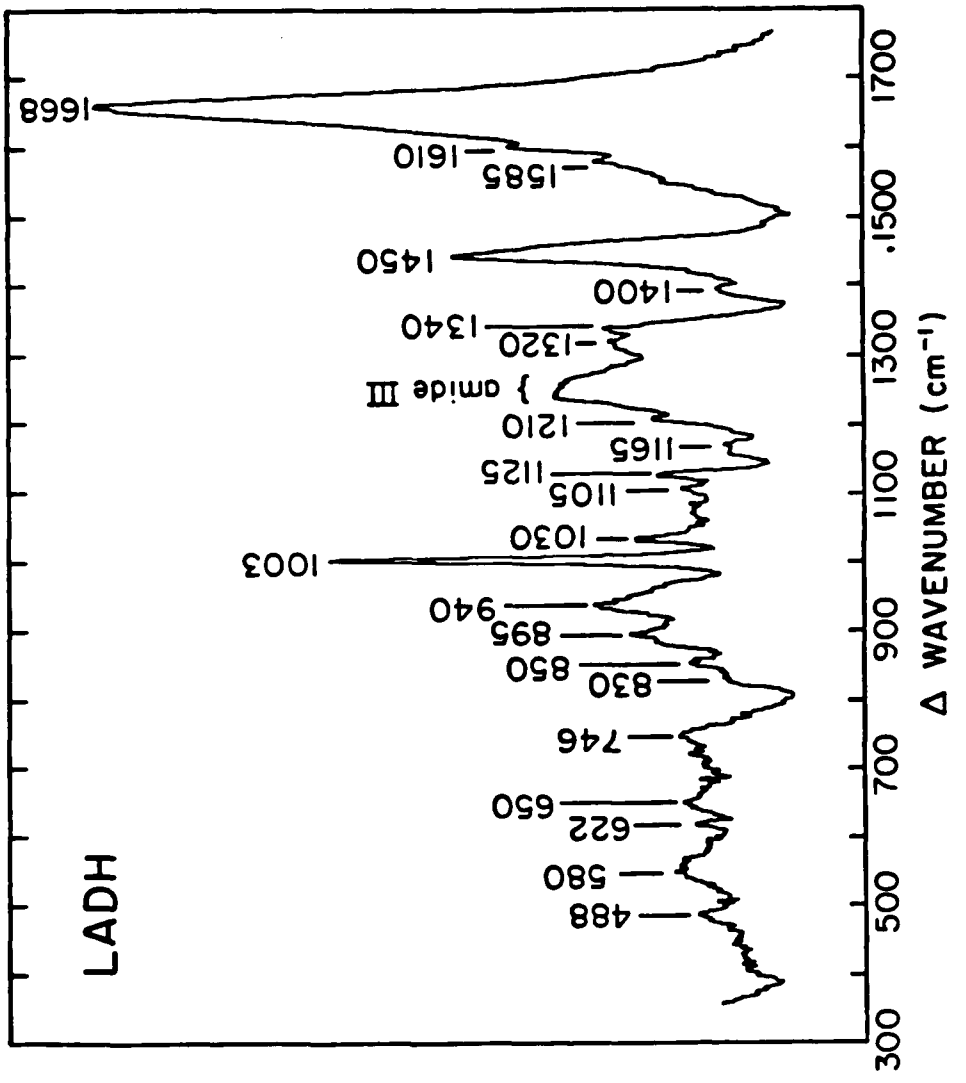
LADH
1668
1610
1585
1450
1400
1340
1320
} amide III
1210
1165
1125
1105
1030
1003
940
895
850
830
746
650
622
580
488
300
500
700
900
1100
1300
1500
1700
Δ WAVENUMBER (cm⁻¹)

Figure 4.

Table 1: Principal peak frequencies in the Raman spectrum of liver alcohol dehydrogenase (Fig. 4).

Peak Frequency (cm^{-1})	Tentative Assignment
488	
580	
622	Phe ring mode
650	
746	
830^{sh}	Tyr
850	Tyr
895	
940	
1003	Phe
1030	Phe
1105	
1125	C-C stretch in hydrocarbon
1165	Phe, Tyr
1210	Phe, Tyr
1230^{sh}	Amide III: β-sheet
1245	Amide III: random coil
1265^{sh}	Amide III: α-helix
1320	
1340	γ-CH_2
1400	Asp, Glu: COO^-
1450	δ-CH_2
1585	Phe, Arg
1610	Phe, Tyr
1668	Amide I p

Figure 5: Raman spectrum of LADH in D_2O buffer (0.1 M pyrophosphate buffer pD 9.6). Incident power was 170 mW with all other conditions being the same as in Figure 4.

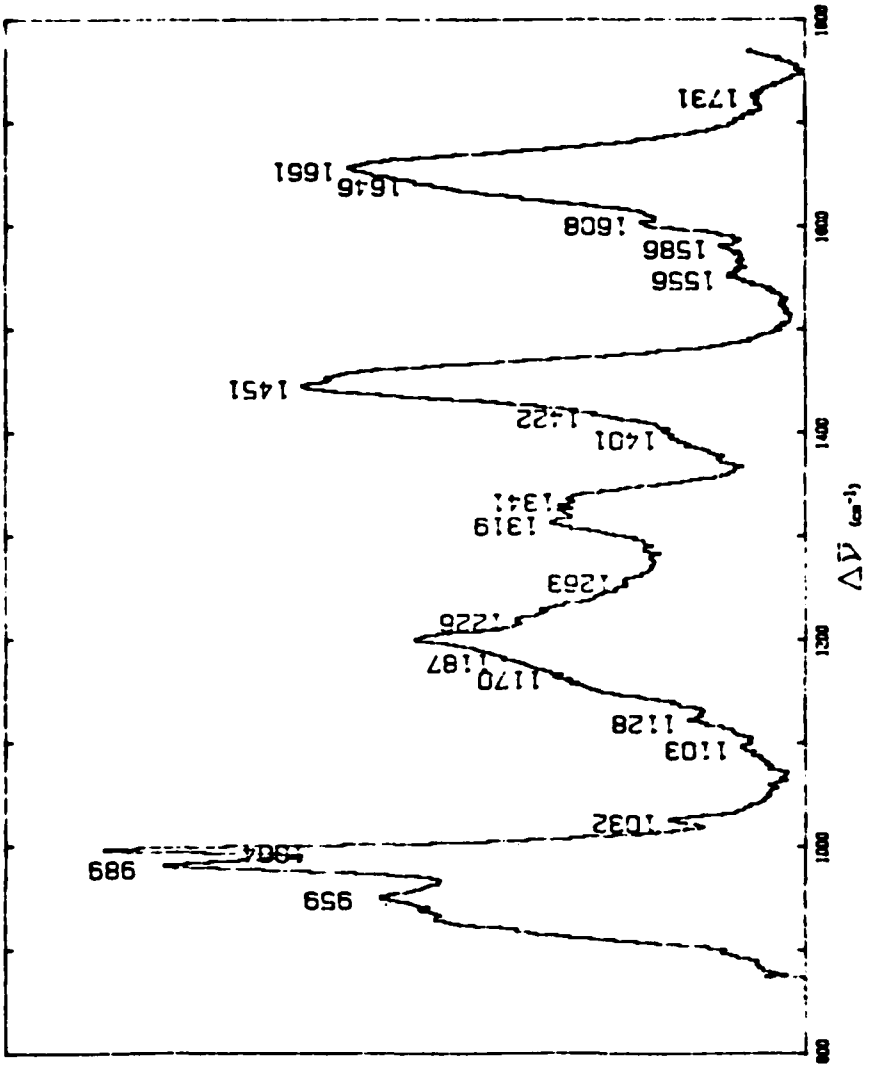
1731
1646
1661
1608
1586
1556
1451
1422
1401
1341
1319
1263
1226
1187
1170
1128
1103
1032
989
959
1800
1600
1400
1200
1000
800
$\Delta\tilde{\nu}$ (cm^{-1})

Figure 5.

amide vibrations are known to be sensitive to the secondary structure of the proteins (19,22,108). Typical ranges for these bands are: for amide I, 1645-1660 cm^{-1} for α helix, 1665-1680 cm^{-1} for β sheet and 1660-1670 cm^{-1} for unstructured random coil; for amide III, 1265-1300 cm^{-1} for α helix, 1230-1240 cm^{-1} for β sheet and 1240-1260 cm^{-1} for random coil. Various methods have been used to calculate the percentages of each type of structure (52,73,101,102). Lippert et al. (52) defined the intensities at three frequencies which are indicative of three types of secondary structure: 1240 cm^{-1} (amide III) for β-sheets; 1632 cm^{-1} (amide I') for α helix and 1660 cm^{-1} (amide I') for random coil. Typical intensities for each type of structure at these frequencies were obtained from model polypeptides and proteins with known structure. The sum of the intensities for the different types of structures scaled down by its corresponding percentages gives the observed Raman intensity. Percentages of each type of structure were calculated by solving the simultaneous equations. Following this procedure, we found that LADH in solution contains 21% α helices, 35% β-pleated sheets, and 43% of unstructured random coil. These percentages are close to the structure obtained by X-ray crystallography (29% helix, 34% β-pleated sheet and 37% random coil; Eklund et al., 1976). Following a simplified method of Williams et al., (101) which uses a calculation of structure based only on the amide I bands, a low percentage of α helix (18%) was also obtained. The small difference in helical structure as

determined by the X-ray and Raman techniques may be indicative of small conformational changes that occur upon dissolving the crystals into this buffer solution or in crystallizing a soluble protein.

In addition, we have been unable to detect any pH dependence of the Raman spectrum of LADH from pH 7.0 to 9.6. A pH dependent conformational change in the LADH structure defined by a pK of 9.8 was postulated previously (104). At pH 9.6, there exists approximately 40% of the deprotonated form whereas none of this form is present at pH 7.0. The Raman spectra of LADH at these two pH's are identical to within less than 3%. Measurements at pH values higher than 9.6 were precluded because LADH denatures under these conditions. Nevertheless, we conclude that over the pH range of 7.0 - 9.6, only small changes in the secondary (or tertiary) structure of LADH occurs and that these changes are not detectable by Raman spectroscopy.

Studies of binary complex LADH/NADH

Recently, we developed a methodology via which very accurate Raman difference spectra can be obtained. Apriori, it may seem unlikely that the classical Raman spectrum of adenine, a 137 MW molecule, can be distinguished from that of LADH, with a monomer of 40,000 MW. As a matter of fact we have demonstrated in our lab that the classical Raman spectrum of adenine bound to the active site of LADH can be obtained. Two prominent reasons why these experiments are possible are: 1) The classical Raman bands observed from proteins are broad compared to nucleotide bands. For example, the amide I protein band is some 100 cm^{-1} wide compared to the 10 cm^{-1} width of a typical adenine band. This suggests that we gain a factor of 10 in relative peak intensities of adenine versus protein over a simple comparison of molecular weights. Taking the relative peak intensities of nucleotide to protein bands to scale according to relative molecular weight and inversely to peak width, we expect to find $I_{adenine}/I_{protein} \sim 4\%$. We find, experimentally that the ratio is on the order of 2-7% depending on which adenine and which protein band are being compared. 2) The optical multichannel analyzer (OMA) detection system is highly sensitive relative to the photomultiplier tube detection device and is much more immune to spectrometer drift. This means that one gets a better signal-to-noise so that very sensitive difference spectra can be obtained when one subtracts a protein spectrum from a spectrum of the protein-dinucleotide

complex. In addition, because the spectrum is taken all at once with the OMA device it is possible to take the spectra of samples in an interleaving manner (defined as $A_1B_1B_2A_2A_3...B_nA_n$). Such an approach compensates for spectrometer drift, since the spectrometer drift will tend to affect the sum of all the A measurements in the same way as the sum of the B measurements and subtract out of the difference of these two. With this methodology, very sensitive Raman difference spectrum for NADH bound to LADH was obtained.

Figure 6 shows the Raman spectrum of LADH (Figure. 6b) and its binary complex with NADH (Figure. 6a). It is clear that most of the Raman scattering of the binary complex is due to LADH. In fact, the intrinsic Raman cross section of NADH is only a few percent of that of LADH; the strongest peak of NADH in solution at 1688 cm^{-1} is about 10% of the 1450 cm^{-1} peak of LADH. In order to obtain the Raman spectrum of bound NADH, difference spectra were calculated. It is known that binding of NADH quenches the fluorescence of LADH (55,92). High pH can also quench fluorescence (104). At pH 9.6, the Raman spectrum of LADH and that of the binary complex have only slightly different fluorescence backgrounds. The backgrounds were removed, and any difference in concentration or collection optics between the two samples was corrected by comparing the peaks at 1450 cm^{-1} (52,110). The 1450 cm^{-1} peak, which is due to the α-CH_2 vibration, is a convenient reference because it is relatively insensitive to different

Figure 6: (a) Raman spectrum of the binary complex LADH/NADH. Concentration of LADH:NADH = 1:2 mM. (b) Raman spectrum of LADH. Concentration = 1.3 mM. Samples were maintained at 4 °C, incident power was 100 mW with all other conditions being the same as in Figure 4.

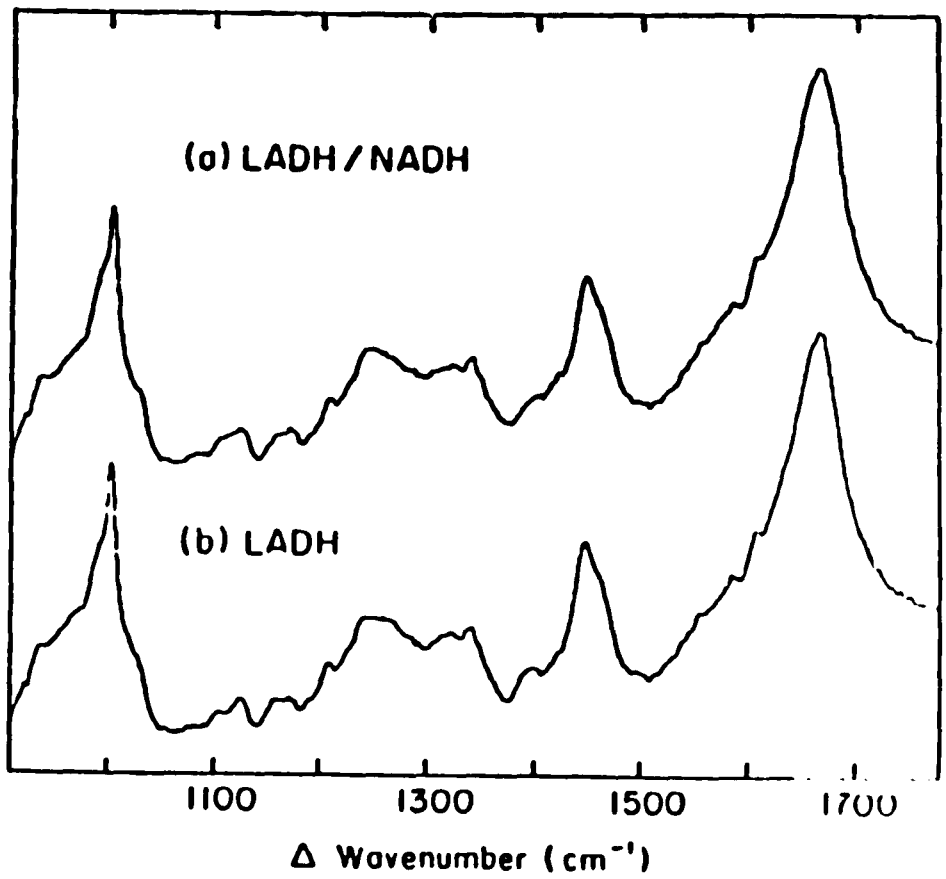

Figure 6.

secondary and tertiary structures of the protein (52). In addition, there is no peak in the Raman spectrum of NADH in buffer solution around this region. The resulting difference spectrum is shown in Figure 7a. There is a small residual broad peak around 1650 cm^{-1} due to different contributions of water in the original spectra. Figure 7b shows a typical Raman spectra of NADH in buffer solution for comparison.

The difference spectrum is due to either bound NADH or conformational changes in LADH when NADH binds. There is no obvious negative peak (which can only be due to LADH changes), suggesting that the LADH spectrum does not change upon binding. As discussed above, changes in protein structure will appear as changes in the Raman spectrum in the amide I and/or amide III vibrations at 1645-1680 cm^{-1} and 1230-1300 cm^{-1} regions respectively. That there are no negative peaks nor obvious 'new' peaks in these regions suggests that the change in the structure of LADH upon NADH binding is small. The difference spectra in Figure 7a is due, probably entirely, to bound NADH. Recent measurements of ADPR bound to LADH's active site have confirmed this (23).

Several obvious changes can be seen when NADH binds to LADH as compared to that in solution. The most prominent change is the disappearance of the major peak in the solution spectrum at 1545 and 1338 cm^{-1}. The broad 1545 cm^{-1} band has been assigned to the nicotinamide moiety (12,76;see next section). The disappearance of

Figure 7: (a) Difference Raman spectrum of spectra (a) and (b) of Figure 6 showing basically bound NADH. The peak around 1685 cm^{-1} was arbitrarily adjusted to be about the same height in both panels. (s) = solvent. Conditions of both spectra are the same as above (Figure 4). (b) Raman spectrum of NADH in solution. Concentration = 32 mM.

Figure 7.

(a) Bound NADH
(b) Free NADH in solution
Raman Intensity
Δ Wave Number (cm⁻¹)
300
500
700
900
1100
1300
1500
1700
391
510
716
(S)
1087
1114 (P)
1172 (A)
1198
1245 (N,A)
1303 (A)
1324 (A)
1340 (A)
1375 (A,N)
1415 (N)
1510 (A)
1575 (A)
1600 (N)
1616 (N)
(S)
1681
(N)
390 (N)
526 (A,N)
730 (A)
830 (P)
918 (P)
940 (N)
998
1084 (P,N)
1112 (P)
1182 (N)
1246 (N,A)
1308 (A)
1338 (A)
1378 (A,N)
1422 (N,A)
1458 (N)
1546 (N)
1578 (A)
1618 (N)
1688 (N)

the 1545 cm^{-1} band shows clearly that the nicotinamide moiety is directly involved in the binding of NADH by LADH. The 1338 cm^{-1} band also has apparently disappeared. It is well known that the 1338 cm^{-1} band is due to a ring mode of the adenine moiety (51,53,76). The disappearance of this band supports the fact that the adenine part of NADH is directly involved in binding.

The broad feature around 1080 cm^{-1} in the spectrum of NADH in solution has been assigned to the NH_2 rock (12). NADH contains two NH_2 groups, one associated with the nicotinamide ring and another with the adenine ring. As expected, the band shifts to around 900 cm^{-1} upon deuteration of NADH (Figure 8), while the peak at 1109 cm^{-1}, which is not assigned to the NH_2 groups, remains unchanged. The solution spectrum peak at 1080 cm^{-1} of Figure 7b shifts to 1087 cm^{-1} with reduced intensity and appears to narrow upon forming the binary complex, Figure 7a. It is thus likely that at least one of the two NH_2 groups in NADH is directly involved in binding, disrupting the rocking motion of NH_2.

There are other changes in the relative intensities of several bands. For example, the relative intensity of the 1418 and 1688 cm^{-1} bands of NADH in solution remains relatively unchanged upon binding, as do the 1307 and 1377 cm^{-1} bands. However, the ratio of the 1418 (1688) cm^{-1} to 1307 (1377) cm^{-1} band is considerably reduced when NADH binds to LADH.

NADH exists in two possible configurations in polar solvent (21,27,59,60,71). At 22°C, there is a minimum of 30-40% of the

Figure 8: Raman spectrum of (a) NAD^+ (62 mM) and (b) NADH (41 mM) in 0.1M phosphate D_2O/buffer (pD 7.0). Other conditions are as in Figure 7.

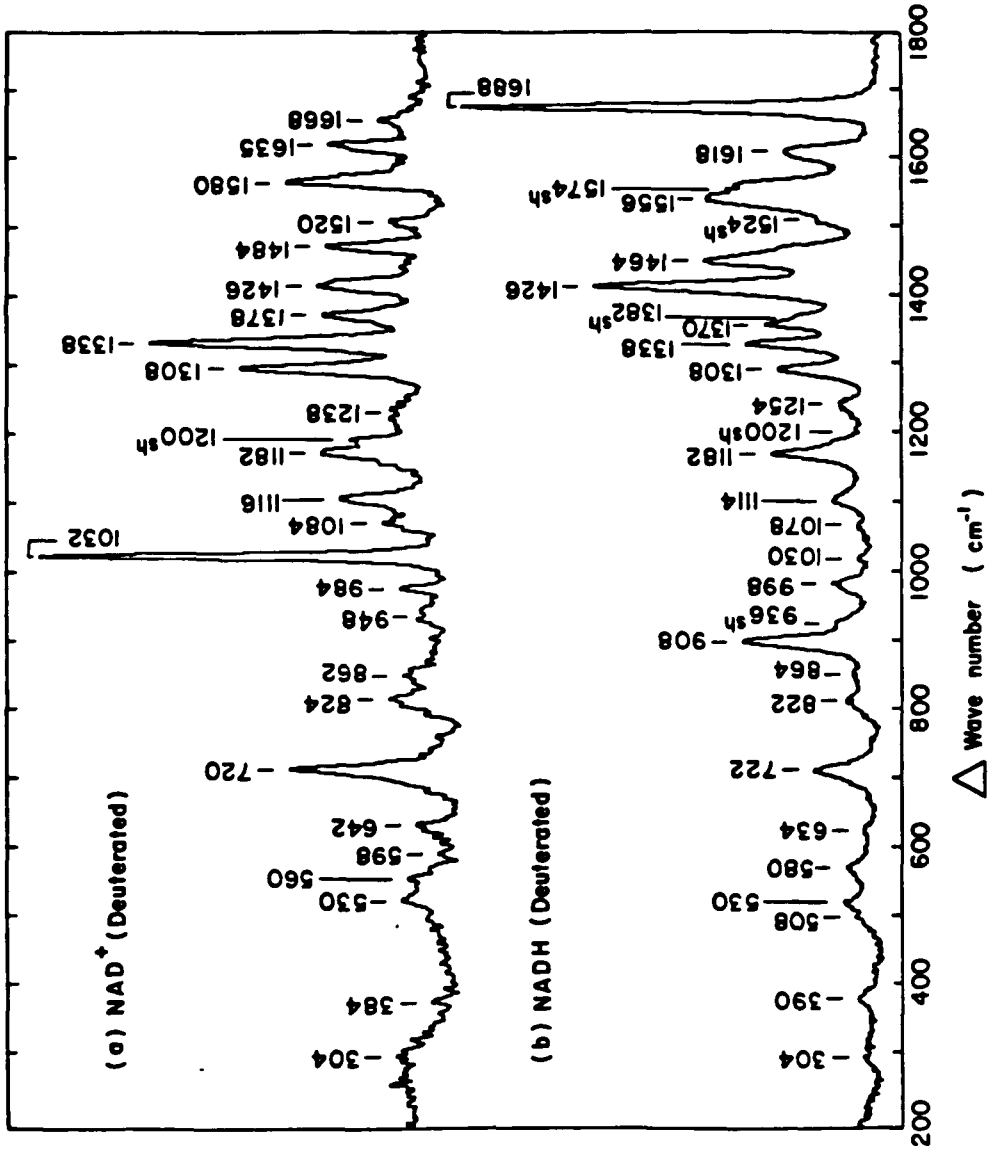
(a) NAD+ (Deuterated)
1032
1668
1635
1580
1520
1484
1426
1378
1338
1308
1238
1200sh
1182
1116
1084
984
948
862
824
720
642
598
560
530
384
304
(b) NADH (Deuterated)
1688
1618
1574sh
1556
1524sh
1464
1426
1382sh
1370
1338
1308
1254
1200sh
1182
1114
1078
1030
998
936sh
908
864
822
722
634
580
530
508
390
304
200
400
600
800
1000
1200
1400
1600
1800
Wave number (cm-1)

Figure 8.

folded form in solution where the adenine ring is stacked with the nicotinamide ring (70). At higher temperature or in a nonpolar/destacking solvent such as methanol, NADH exists mainly in an open form whereas LADH-bound NADH exists entirely in the open form (37). Raman spectra of NADH at 25°C and 75°C (where there is no stacking) were measured, and they are essentially the same. Thus, the observed stacking of NADH in solution has only minimal effect on the Raman spectrum or perhaps the changes in conformation is not picked up by Raman.

The adenine moiety is known to be important for the binding of NADH to LADH. NADH fragments without the nicotinamide ring can bind to LADH and X-ray crystallographic studies (1,37,74) showed that adenine binds in a cleft in the coenzyme binding domain of LADH. Difference ultraviolet (88) and NMR studies (43) also indicated that the adenine moiety is perturbed by binding.

The role of the nicotinamide moiety of NADH in binding has been studied less extensively. There is clear indication from X-ray studies that the nicotinamide ring interacts with specific amino acid residues on LADH. However, Hollis (43) has suggested that both adenine and nicotinamide rings are bound in the binary complex. By monitoring the NMR spectra of protons in NADH in D_2O buffer, he concluded that the nicotinamide moiety is affected by binding. In addition, Subramanian & Ross (86,87) studied the calorimetry of NADH and NAD^+ binding for various dehydrogenases and found that there are large entropy changes only when NADH or

NAD^+ binds to LADH. They noted further that binding of ADPR, a fragment without the nicotinamide part, to LADH does not result in a large entropy change. Futhermore, LADH forms orthorhombic crystals normally, but the binary LADH/NADH complex (and almost all ternary complexes of LADH/NADH with various substrates or inhibitors) cannot form orthorhombic crystals. In contrast, many NADH fragments, which do not contain nicotinamide, form orthorhombic crystals with LADH (13,112). It is thus possible that the nicotinamide moiety or the entire NAD structure is promoting the activity of LADH by forcing a conformational change on the enzyme (9).

Moreover, Samama et al. (79) have shown that the carboxamide group of the nicotinamide moeity is crucial for the correct binding of NAD^+ to LADH. X-ray studies indicated that the analogue of NAD^+ without the carboxamide group binds LADH with the adenine moeity in the same way as NAD^+ but the pyridine moiety is in a different position, further away from the active site. Studies on other dehydrogenases have also revealed some interactions of the carboxamide group with amino-acid residues on the enzyme, possibly with a histidine group (3,99). Woenckhaus et al. (1973) studied the binding of the analogue [3-(3-bromoacetylpyridine)propyl]-adenosine pyrophoshate to yeast alcohol dehydrogenase and showed a direct bonding between the carboxy-methyl group and a histidine residue.

The Raman spectrum of bound NADH indicates that both adenine and nicotinamide parts are directly involved when NADH binds to

LADH. The 1338 cm^{-1} peak associated with the adenine moiety and the 1545 cm^{-1} peak due to the nicotinamide moiety, found in solution spectrum of NADH, disappear in the LADH/NADH complex. In addition, at least one of the two NH_2 groups is also perturbed. Since the 1545 cm^{-1} peak is sensitive to the carboxamide, its disappearance is also consistent with a direct involvement of the carboxamide group.

Studies of $NAD^+$and NADH Fragments

In order to understand the Raman spectra of NADH and NAD^+ in solution and when bound to the active site of LADH, we undertook an extensive study on adenine, adenosine, AMP, ADP, ADPR, NMN^+, NMNH, 1-methylnicotinamide iodide, 9-ethyladenine, and 3-$PAAD^+$. In addition to studying these fragments and analogues of NADH and NAD^+ the effects of pH and the deuteration of the exchangable protons on the Raman spectra of NADH, NAD^+, their fragments and analogues were studied as well. In this way we were able to identify the bands of the Raman spectra of NADH and NAD^+ with specific moieties of these compounds. The Raman spectra of NAD^+ and NADH at pH 7.0 are shown in Figure 9b and 10b respectively. The Raman spectra of the two major fragments of NAD^+ and NADH (NMN^+ or NMNH and AMP; see Figure 11 for the diagrams of molecules) are also shown in Figure 9 and 10. It is clear that peaks in NAD^+ and NADH spectra can be identified as being from either NMN^+/NMNH or the AMP moiety. Measurements of equimolar concentrations of NMN^+/NMNH and AMP when added reproduced respectively the spectra of NAD^+ and NADH very well. The small differences in the summed spectra when compared to the NAD^+ or NADH spectra are presumably due to peaks which can be easily assigned to structural changes due to the joining of the two fragments. This shows that the two major fragments are basically independent of each other with regards to their Raman spectra. From measurement of known mixtures of NAD^+ and NADH, it was

Figure 9: Raman spectrum of (a) AMP (110 mM), (b) NAD^+ (45 mM), and (c) NMN^+ (78 mM) in 0.1M phosphate buffer (pH 7.0) at room temperature. Laser line was 488 nm with 100 mW incident power, and the resolution was 8 cm^{-1}. The spectrum of AMP was amplified by a factor of 5/3 for clarity. As taken on the scanning apparatus, each spectrum consists of 800 channels with an effective dwell time of 4 seconds/channel. Thus, each spectrum took about an hour to take. The reticon spectrometer (see Methods) is about 100 times faster.

(a) AMP
324
394
438
538
572
642
730
804
822
854
882
910
980
1000
1040
1084
1130
1176
1220
1254
1308
1338
1378
1422
1462
1484
1510
1580
1652
(b) NAD+
326
538
564
642
732
802
834
854
888
914
1034
1086
1116
1186
1224
1256
1308
1340
1382
1422
1458
1484
1510
1582
1628
1700
(c) NMN+
386
540
640
800
888
980
1032
1106sh
1134
1190
1258
1424
1460
1508
1590
1630
1700
200
400
600
800
1000
1200
1400
1600
1800
Wave number (cm-1)

Figure 9.

Figure 10: Raman spectrum of (a) AMP (110 mM), (b) NADH (67 mM), and (c) NMNH (16 mM). Conditions are as in Figure 6. The spectrum of AMP was amplified by a factor of 2.5 for clarity.

(a) AMP
324
394
438
538
572
642
730
804
822
854
882
910
980
1000
1040
1084
1130
1176
1220
1254
1308
1338
1378
1422
1462
1484
1510
1580
1652
(b) NADH
324
390
526
568sh
632
728
830
850sh
878
918
940
998
1082
1112sh
1182
1228sh
1246
1308
1338
1378
1420
1458
1482
1514sh
1546
1578
1618
1688
(c) NMNH
390
524
790
878
944
988
1084
1186
1240
1302
1382
1422
1458
1546
1618
1634sh
1690
200
400
600
800
1000
1200
1400
1600
1800
Wave number (cm⁻¹)

Figure 10.

Figure 11: Schematic of NADH, NAD^+. NMNH, $1\text{-}MN^+$, NMN^+, AMP, and 9EtAd. N, nicotinamide; R_2, ribose next to N; P, phosphate; R_1, ribose next to adenine; A, adenine.

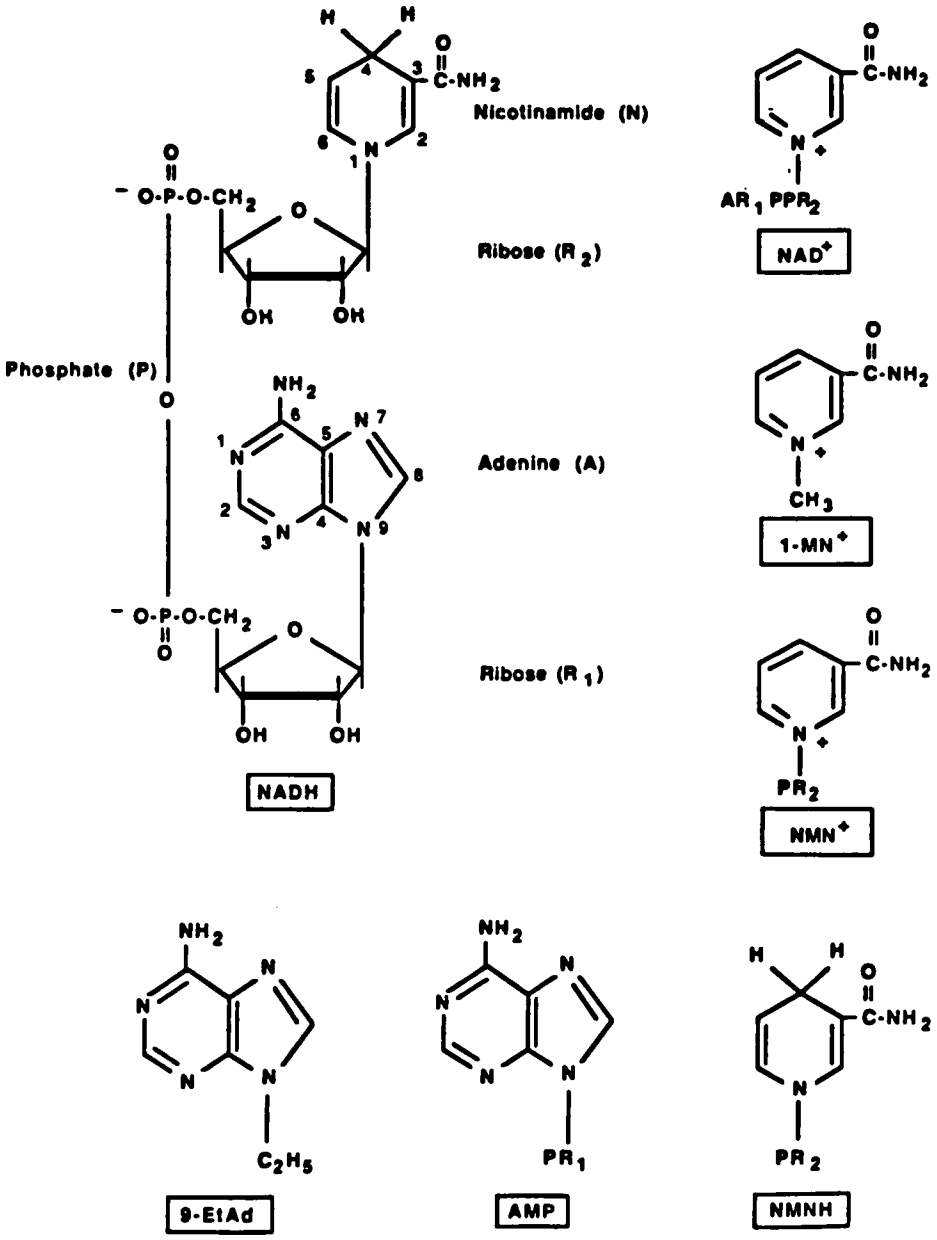
Nicotinamide (N)
Ribose (R_2)
Phosphate (P)
Adenine (A)
Ribose (R_1)
NADH
AR_1PPR_2
NAD^+
CH_3
$1\text{-}MN^+$
PR_2
NMN^+
C_2H_5
9-EtAd
PR_1
AMP
PR_2
NMNH

Figure 11.

observed that the intensity of the 1338 cm^{-1} peak, due to the adenine moiety (see below), is the same in NADH and NAD^+ as expected.

Table 2 summarizes all the major band positions and relative band intensities in the fragments and analogues of NADH/NAD^+ at pH 7.0. The intensities were calculated relative to the 1338 cm^{-1} adenine band (arbitrarily set to 10), whenever it is present, and indirectly through the peak at 1688 cm^{-1} of NADH or the peak at 1032 cm^{-1} of NAD^+ for fragments not containing adenine.

Assignments of the major peaks of NADH and NAD^+ to a particular group is based mainly on the peak's presence in the corresponding fragment spectrum containing the moiety with about the same intensity. For example, the peak at 1308 cm^{-1} is assigned to adenine since it is observed in the spectra of all adenine containing fragments and is not present in fragment spectra where adenine is absent. Likewise, the peak at 1032 cm^{-1} is assigned to molecular motions in the oxidized nicotinamide moiety since this band is present in the spectra of all fragments containing oxidized nicotinamide. Further assistance in the assignments comes from the pH dependences and deuteration effects of the various bands. Table 3 summarizes the assignments of all the major peaks in NADH and NAD^+ spectra obtained in this way. Rodgers and Peticolas (76) previously assigned many of the bands in the resonance Raman spectrum of NADH using resonance Raman techniques. In general, the agreement between their study and the

Table 2. Raman peak frequencies (cm^{-1}) and relative intensities (in parenthesis) of adenine, 9EtAd, adenosine, AMP, ADP, ADPR, NMNH, NMN^+, and 1-MN^+ in pH = 7.0 buffer.

adenine	9EtAd	adenosine	AMP	ADP	ADPR	NMNH	NMN^+	1-MN^+
302(1)	333(3)	316(1)	324(1)	324(2)	328(3)			
	391^{br}(1)		398^{br}(0)			390(3)	386(1)	371(1)
			438^{br}(0)	810(1)				810^{br}(1)
				856(2)				862^{br}(1)
						524^{br}(8)		
539(3)	531(2)	538(2)	536(1)	538(1)	538(2)		540^{br}(1)	530(3)
	582(1)		572^{br}(1)	552(4)	560^{sh}			551^{sh}
622(3)					632^{br}(1)			
		630^{br}(1)	642(1)	640(1)			640^{br}(1)	633^{br}(1)
	713.5(4)							
722(11)	731.5(9)	730(8)	730(5)	732(6)	732(6)			735(4)
				788(7)		790(2)		
	802(2)		804(1)		802(6)		800(2)	
			822(1)	826(1)	830^{sh}			
			854(1)	850(3)	850^{sh}			
872(2)	876(2)	868(2)	882(1)	883(3)	883(4)	878(6)	885(1)	
	912(1)	910^{br}(1)	910(1)	910^{sh}	910^{sh}			
948(3)	951^{sh}					944(4)		
			980(3)				993(4)	
990(4)	991(4)	990(2)				985^{br}(8)		990(1)
			1000(2)					
		1008^{sh}						
			1040(1)	1035(5)			1032(15)	1034(15)
1079(1)	1079(2)		1084(1)	1080(3)	1078(4)	1084^{br}(9)		
	1091(2)							
				1110(2)			1106^{sh}	
1121(1)		1132(1)	1130(0)		1116(3)			
1143^{sh}							1134(2)	
		1178(1)	1176(1)	1182(1)	1178(1)			
						1186(4)	1190(2)	
	1196^{br}(2)							
								1217(2)
		1214(2)	1220(1)	1228^{sh}	1230^{sh}			
						1240(4)		
1249(3)	1254(2)	1258(2)	1254(2)	1266(4)	1252(3)		1258^{br}(1)	
	1279(3)							
								1300^{br}(0)
1309(6)	1311(6)	1308(7)	1308(6)	1310(6)	1308(7)	1302(3)		
1330(10)	1335(10)	1338(10)	1338(10)	1340(10)	1340(10)			
1363(4)	1368(6)	1378(4)	1378(4)	1380(5)	1382(6)	1382(6)		
1396(3)								
1419(2)	1418(2)	1428(2)	1422(2)	1426(2)	1428(4)	1422(13)	1424(3)	1418(3)
	1451(3)			1450(4)				
	1463^{sh}		1462(1)		1462(3)	1458(7)	1460(2)	1471^{sh}
1485(5)	1489(1)	1486(3)	1484(3)	1486(4)	1486(5)			
1497^{sh}								
	1516(3)	1512(3)	1510(3)	1512(3)	1510(5)		1508^{br}(0)	1511(0)
						1546^{br}(15)		
1569^{sh}								
	1580(3)	1582(5)	1580(4)	1584(5)	1584(7)			
							1590(3)	1595(2)
1596(7)								
						1618(8)		
	1640^{br}(2)		1652^{br}(1)	1656^{br}(1)	1646^{br}(1)	1634^{sh}	1630^{br}(3)	1632^{br}(2)
						1690(25)	1700(1)	1692(1)

sh: shoulder; br: broad

Table 3: Assignment of Peaks in the Raman Spectrum of NADH and NAD+ (relative intensity in parenthesis).

Peak frequency (cm^{-1}) NAD$^+$	NADH	Assignment[a]
324^{br}(2)	324^{br}(3)	P
	390(3)	N
538(1)	526^{br}(4)	A for NAD$^+$; .2A + .8N for NADH
564^{br}(1)	568^{sh}	P/R
642^{br}(2)	632^{br}(2)	.5A/R_1 + .5N for NAD+; A/R_1 for NADH
730(7)	730(7)	A/δR_1
800(0)		R_2/N
834(2)	830^{br}(2)	P
854(1)	850^{sh}	R_1/P
888^{br}(2)	878(3)	P
914(2)	918(3)	P
	940(4)	N
	998(4)	N
1032(15)		N
1084(3)	1034(9)	P for NAD$^+$; .3P + .7N* ($-NH_2$) for NADH
1116(4)	1112^{sh}	R_2/pyrophosphate
	1182(5)	N
1186^{br}(3)		R_2/N
1224(3)	1228^{sh}	P
1254(4)	1246(5)	A* for NAD$^+$; .8N* + .2A* for NADH
1308(7)	1308(7)	A
1338(10)	1338(10)	A/δR_1
1378(6)	1378(9)	A/R_1 for NAD$^+$; .7A/R_1 + .3N* for NADH
1422(5)	1422(17)	.5A/δR_1* +.5N* for NAD$^+$; .1A/δR_1* + .9N* for NADH
1458(3)	1458(8)	R_2/δN
1484(4)	1484(4)	A
1510(4)	1514^{sh}	A/δR_1
	1546(16)	N*
1580(6)	1578^{sh}	.8A/δR_1 + .2N for NAD$^+$; A/δR_1 for NADH
	1618(9)	N
1628^{br}(3)		N*
	1688(25)	N
1700(1)		N*

br: broad, sh: shoulder, *: deuteration effect, P: phosphate, A: adenine, N: nicotinamide, R: ribose (R_1 near A; R_2 near N), δ: small influence. Modes involving more than one moiety are indicated by symbols separated by a slash. Peaks containing two separate degenerate or nearly degenerate modes are indicated by + sign separating the two modes with the relative contribution in intensity in front of the symbol.

present study is excellent.

Adenine related peaks: The Raman spectrum of the adenine moiety (with and without the ribose and/or phosphate) has been studied extensively, mainly in conjunction with the other bases found in nucleic acids (51,53,75). More recently, pre-resonance and resonance Raman studies of adenine were reported (16,24,40,50,67). In general, the assignments in this report agree with these results. The 1308, 1338, 1378, 1422, 1484, 1510, and 1580 cm^{-1} bands in NAD^+ are known as ring modes for adenine. These results show that some of these modes, namely the 1338, 1378, and 1422 cm^{-1} bands, are at slightly different frequencies in the spectrum of adenosine, indicating that these modes are affected by the ribose, R_1, in various degrees. The 1510 cm^{-1} and 1580 cm^{-1} bands are not present in the adenine spectrum but similar peaks to those found in adenosine are observed in the 9-ethyl adenine spectrum. Peaks at 538 cm^{-1}, 642 cm^{-1} and 730 cm^{-1} are also due to adenine, with the 730 cm^{-1} peak affected to a degree by the ribose.

All of these modes are also present in the spectrum of NADH. Some peaks appear to have different intensities because of the presence of additional bands due to the reduced nicotinamide moiety with very close, or identical, frequencies (see Table 3). For example, the 538 cm^{-1} adenosine peak is apparently unresolved in the broad 526 cm^{-1} peak of NADH since the broad peak contains contribution of a peak at 526 cm^{-1} coming from the reduced

nicotinamide moiety. Similarly, the 1378 and 1422 cm^{-1} peaks of NADH have significant Raman contributions from nicotinamide related modes in addition to those from adenosine. The labelled peak at 1246 cm^{-1} in the NADH spectrum would appear to consist of the 1254 cm^{-1} adenine related band the 1240 cm^{-1} nicotinamide related band.

Nicotinamide related peaks: The nicotinamide ring structures of NAD^+ and NADH are very different and thus yield very different Raman spectra (e.g. contrast NMN^+ and NMNH in Figures 9c and 10c). The Raman spectrum of NAD^+ is very similar to that of ADPR, indicating that the oxidized nicotinamide moiety does not contribute much to the spectrum of NAD^+. The major exception to this is a mode at 1032 cm^{-1}, a prominent peak in the NAD^+ (and the NMN^+) spectrum. This can clearly be assigned to an aromatic ring "breathing" mode, (envisioned as a "contraction and expansion" of the ring) of oxidized nicotinamide. There are also two smaller bands at 800 cm^{-1} and 1186 cm^{-1} (shoulder) in the NAD^+ spectrum; these are due to molecular motions located on the nicotinamide moiety as well as the ribose, R_2. Peaks at 642, 1422, and 1580 cm^{-1} have substantial contributions from bands due to nicotinamide at similar positions in addition to adenosine. The broad peak at about 1628 cm^{-1} is also due mostly to nicotinamide; however, some of this mode's intensity arises from adenine since adenine also has a weak broad peak at that position. Many investigators have reported different values for the highest frequency mode observed in the Raman spectrum of NAD^+, which is attributed to the C=O

stretch (8,41,65). In this study a small shoulder at 1700 cm^{-1} in the NAD^+ spectrum, which may have been neglected in some of these earlier studies, has consistently been observed. This band is clearly visible if the contribution due to water/buffer is subtracted, as in Figure 9b. The results of this study discussed below indicate a substantial deuteration effect in the 1700 cm^{-1} mode, making it unlikely that this is due to be a simple C=O stretching mode.

In contrast to NAD^+, the reduced nicotinamide moiety yields many prominent peaks in the NADH spectrum. By comparing the Raman spectrum of NADH and NMNH, it is easy to identify the bands at 390, 526, 940, 1084, 1182, 1378, 1422, 1546, 1618, and 1688 cm^{-1} as due to the nicotinamide moiety. The peak at 1084 cm^{-1} has been assigned to the rocking motion of $-NH_2$ of the amide (ref. 12, also see discussion above). Upon deuteration, it shifts down to 908 cm^{-1} as previously mentioned. The strong 1688 cm^{-1} band has often been attributed to the C=O carbonyl stretch (8,12,41,65,72). This assignment, however, is seriously questioned (75) in the recent literature.

Peaks due to phosphate: Peaks which appear in the AMP spectrum but not in adenosine's and which also double in intensity in ADP's spectrum, have been assigned to phosphate modes. Further support for these assignments comes from the pH dependencies of these bands. ADP has an apparent pK at 6.3 (4,11) associated with the ionization of the phosphate's last dissociatable proton,

suggesting that NAD^+ and NADH would show similar titration behavior. Indeed titrations of NADH or NAD^+ through pH 6, show significant changes in those bands assigned to the phosphate moiety.

It is important to mention the phosphate band at 1084 cm^{-1} (75) in the spectrum of NAD^+. This band is not visible in NADH because of the much more dominant rocking mode of the amide's $-NH_2$ at 1084 cm^{-1}. Upon deuteration of NADH, however, the phosphate peak is revealed, while the peak due to $-NH_2$ is downshifted to 908 cm^{-1}, as shown above.

Deuteration effects: Figure 8 shows the Raman spectra of NAD^+ and NADH in D_2O/buffer. At pD=7.0, only the two $-NH_2$ groups and the hydroxyl groups of the ribose rings are deuterated. Nevertheless, there are a number of significant changes in the NAD^+ and NADH spectra, despite these apparently relatively minor changes. These indicate that many modes involve motions associated with these $-NH_2$ groups or the ribose moiety to varying degrees. Here in are discussed in turn the changes observed, upon deuteration, for bands assigned to adenine, oxidized nicotinamide ring, reduced nicotinamide ring, and ribose/phosphate moiety. Spectra of deuterated fragments like AMP, NMN^+ and NMNH were also measured to clarify the changes (data not shown). Modes that show a deuteration effect are indicated by an asterisk in Table 3.

The 1422 cm^{-1} peak in both NAD^+ and NADH contains an adenine ring mode which is upshifted slightly by 4 cm^{-1} in D_2O/buffer,

showing that this mode involves the $-NH_2$ group to a degree. The broad peaks at 1246 cm^{-1} for NADH and 1254 cm^{-1} for NAD^+ contain more than one mode. The adenine mode at 1254 cm^{-1} is common in both coenzymes. In D_2O/buffer, this band disappears. (For NADH, a weaker new peak due to the reduced nicotinamide ring appears at about the same frequency in D_2O/buffer). Upon deuteration, two new bands, a shoulder at 1200 cm^{-1} and a peak at 1182 cm^{-1}, appear. Both can be identified with the adenine moiety since similar peaks appear when AMP is deuterated. The 1182 cm^{-1} mode has been assigned to a $-ND_2$ scissor mode by Tsuboi et al. (94) in his studies of adenine. Note that the peak at 1182 cm^{-1} observed in the deuterated NAD^+ and NADH spectra is also partly due to a mode associated with the nicotinamide ring.

A number of spectral changes can be associated with the effects of deuteration upon the oxidized nicotinamide moiety. The broad peak at 1628 cm^{-1} of NAD^+ in H_2O solution is replaced by a peak at 1635 cm^{-1} for deuterated NAD^+. Similar spectral changes occur for NMN^+. The weak peak at 1700 cm^{-1}, in the protonated NAD^+ spectrum, disappears upon deuteration and a new peak at 1668 cm^{-1} appears in D_2O/buffer, suggesting a 32 cm^{-1} downward shift of the 1700 cm^{-1} band upon deuteration. This is not, however, the case. The peak at 1668 cm^{-1} is also present in deuterated NMN^+ but not in any of the adenine containing deuterated fragments, which implies that both peaks are associated with the nicotinamide moiety. However, in the spectrum of 3-PAAD, where the carboxamide

is replaced by an aldehyde, the 1700 cm^{-1} peak is present in H_2O but the 1668 cm^{-1} peak is missing in D_2O/buffer. It is clear that both modes are related to motion of the $-NH_2$ moiety but are separate modes. The weak broad peak at 1258 cm^{-1} in the protonated NMN^+ spectrum, which is part of the observed 1254 cm^{-1} peak in the spectrum of NAD^+, disappears upon deuteration. Correspondingly, a broad peak at 1238 cm^{-1} appears in the deuterated NMN^+ and NAD^+ spectra, suggesting that the oxidized nicotinamide 1258 cm^{-1} mode shifts to 1238 cm^{-1} upon deuteration. The nature of the new broad peak around 948 cm^{-1} in the deuterated spectrum is not clear. However, it is likely to be associated with the nicotinamide moiety since a similar new peak (shoulder) appears in the NMN^+ spectrum in D_2O while no corresponding peak is observed in the D_2O spectra of AMP, ADP, and ADPR.

The most prominent change in the Raman spectrum of NADH in D_2O is the downshift of the 1084 cm^{-1} mode to 908 cm^{-1}. As mentioned above, this mode is associated with the nicotinamide $-NH_2$ rock. The 1240 cm^{-1} NMNH mode, which is part of the observed 1246 cm^{-1} mode in the spectrum of NADH, disappears upon deuteration. A "new" peak due to the nicotinamide moiety appears at 1254 cm^{-1} in the deuterated spectrum. Note that the original 1254 cm^{-1} peak (seen as part of 1246 cm^{-1} side of NADH) in the H_2O spectrum, which is due to adenine moiety, disappears upon deuteration. Similar behavior is observed with the spectrum of NMNH upon deuteration, confirming the assignments made in this report. The 1378 cm^{-1}

peak, due in part mostly to a mode from the reduced nicotinamide moiety (see Table 3), appears to downshift to 1370 cm^{-1}. A shoulder labelled at 1382 cm^{-1} in Figure 8b, is probably due to the 1378 cm^{-1} adenine band, which remains unaffected by deuteration. The corresponding but weaker mode in NAD^+ spectrum, which is due solely to adenosine, is unaffected. In addition, the 1546 cm^{-1} mode is upshifted to 1556 cm^{-1} in D_2O/buffer.

The regions, 300 cm^{-1} to 600 cm^{-1} and 700 cm^{-1} to 900 cm^{-1}, show a number of changes; this is expected as there are many modes due to ribose/phosphate in this region.

pH dependence: No changes in the Raman spectrum of NAD^+ between pH 8.0 to pH 5.0 and NADH between pH 9.6 and pH 7.0 are observed. NAD^+ is not stable at pH higher than pH 8, its Raman signal rapidly disappears irreversibly. For NADH, irreversible changes in the absorption spectrum occur at a pH below about 6. At pH 5.0, for example, the 340 nm absorption peak disappears completely in several hours. Significant changes are also observed in the Raman spectrum of NADH at a pH lower than 6. Between 4.0 and 6.0, all the changes are associated with nicotinamide related peaks. Below pH 4.0, changes in the adenine related peaks are also observed (see below). For example, the intensities of the peaks at 998, 1422, and 1688 cm^{-1} due to nicotinamide are gradually reduced as pH is lowered. The 1688 cm^{-1} peak disappears completely at pH 3. In the meantime, the intensities of the 1618, 1084 and 878 cm^{-1} bands increase,

especially that of the 878 cm^{-1} band, which increases by over 10 fold from pH 7.0 to pH 5.0. Other new bands at 800, 495 and 433 cm^{-1}, also start to appear at pH 5.0 with relative intensities of 4, 4, and 3, respectively. These changes are all probably related to acid denaturation of the reduced nicotinamide moiety.

Major spectral changes occur with the adenine related peaks when the pH is lowered from pH 5.0 for both NAD^+ and NADH. Figure 12 shows the Raman spectrum of NAD^+ at pH 5.0, 4.0, and 3.0. At pH above 5.0, the four peaks associated with the adenine moiety at 1308, 1338, 1378, and 1422 cm^{-1} are easily distinguishable. However, as the pH is lowered, these bands are replaced by the two bands at 1329 and 1411 cm^{-1} at pH 3.0. There are other spectral changes also, which are evident from Figure 12. These spectral changes, which are reversible, are probably associated with the titration of a group with a pK around 3.9 (61). It is likely to be due to a protonation of the adenine ring (15,25,38,48,113). Protonation would clearly cause major changes in the ring modes of adenine as observed. Similar changes are observed in the Raman spectrum of AMP and in the adenine related peaks of NADH as pH is varied from 5 to 3.

Stacking: It is well known that NADH and NAD^+ exist in predominantly folded forms in solution at room temperature, with the adenine and nicotinamide rings stacked together (21,27,59,60,71). The Raman spectrum of NADH at 75°C and with a strong destacking agent, 8M urea has been measured. Under these

Figure 12: Raman spectrum of NAD^+ (66 mM) as a function of pH: (a) pH 5.0; (b) pH 4.0; (c) pH 3.0. Sample at pH 5.0 was in 0.1M phosphate buffer. Phosphoric acid was added to the sample to lower the pH to the desired values. The resolution was 6 cm^{-1}; otherwise conditions are as in Figure 7.

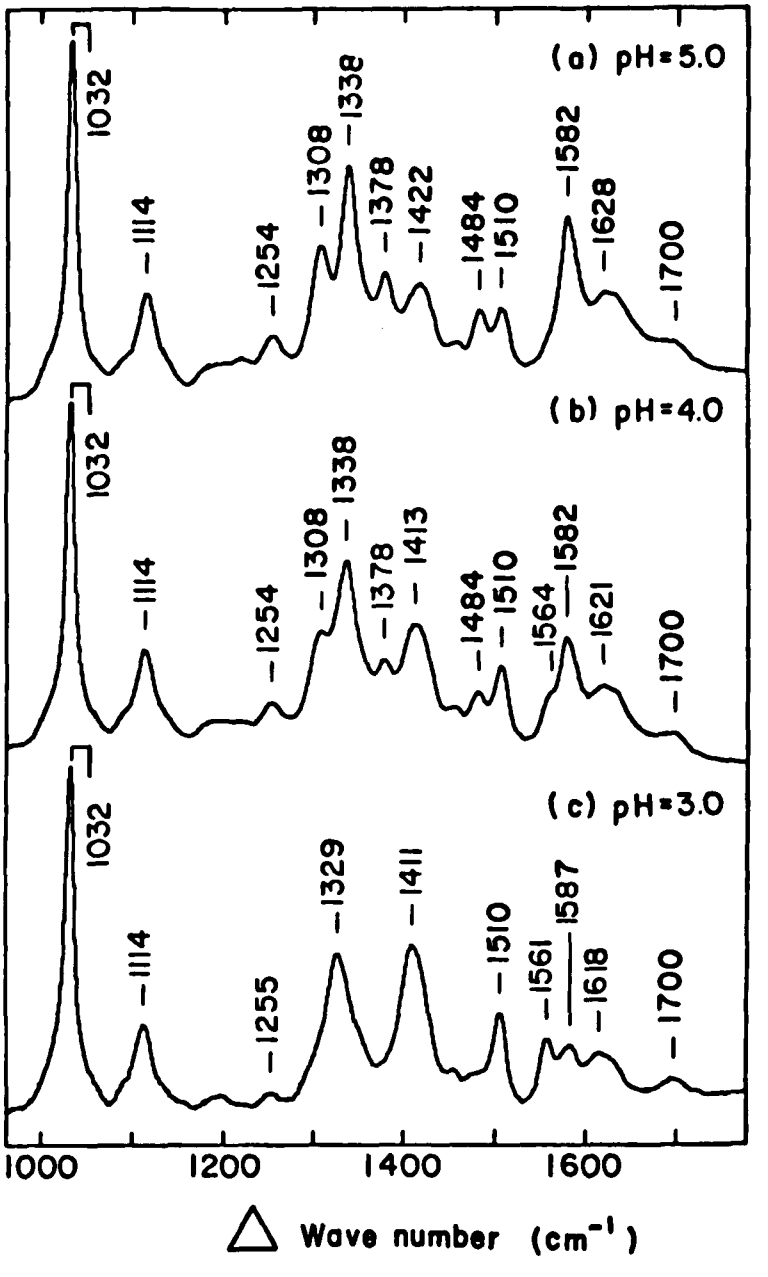
(a) pH=5.0
1032
1114
1254
1308
1338
1378
1422
1484
1510
1582
1628
1700
(b) pH=4.0
1032
1114
1254
1308
1338
1378
1413
1484
1510
1564
1582
1621
1700
(c) pH=3.0
1032
1114
1255
1329
1411
1510
1561
1587
1618
1700
1000
1200
1400
1600
Wave number (cm⁻¹)

Figure 12.

conditions the open form predominates (21,27,59,60). In this work it has been observed the Raman spectra of these two forms are essentially identical with a small downward shift of the peak at 1546 cm^{-1} as the only change. NAD^+ is unstable at high temperatures. However, in 8M urea, no observable changes were seen in the Raman spectrum of NAD^+. Therefore, it is apparent that stacking has no effect on the Raman spectrum of NADH and NAD^+.

Hence, it seems possible to assign the major Raman peaks of NAD^+ and NADH to smaller components of these rather sizable molecules by studying the Raman spectra arising from a series of fragments and analogues. Major changes in the Raman spectrum associated with the adenine moiety are observed when adenine is protonated at pH 3.9. Stacking seems to have a very small or no effect on the Raman spectra of NAD^+ and NADH.

Studies of DABA, its isotopic derivatives and zinc (II) complexes

In our laboratory, binding of the aromatic aldehyde DABA to the substrate binding site of LADH has been successfully detected and its Raman spectrum at the enzyme's active site has been obtained. As a means of understanding the spectroscopic characteristics of DABA in situ we have studied zinc (II) complexes of DABA and isotopic derivatives of DABA as a possible model for that which may occur in the molecular environment of the enzymes active site for this substrate. Furthermore, we have obtained the Raman spectrum of these isotopic derivatives of DABA for the purpose of studying the normal mode pattern of DABA.

Figure 13 shows a schematic representation of the molecular structure of DABA and its isotopically labelled derivatives used in these studies: DABA(CDO), DABA(^{13}CHO), DABA(^{13}CDO) and DABA(2D).

A) Results of, and evidence for the DABA-zinc^{++} model:

For comparative purposes Figure 14 contains the Raman spectrum of: (a) DABA in 0.1M pyrophosphate buffer, at pH 9.6, (b) DABA in situ, and (c) the native DABA in complexation with the zinc ion. The λmax values for these systems are 352, 380 and 372 nm, respectively for DABA in pyrophosphate buffer pH 9.6, when bound to LADH and in complexation with zinc ion in methylene chloride. It is evident from these spectra that the DABA-Zn^{++} complex is fairly representative of that which may be occuring at the active

Figure 13: Schematic representation of the molecular structures of DABA and isotopically labelled DABA(CDO), DABA(^{13}CHO), DABA(^{13}CDO), and DABA(2D).

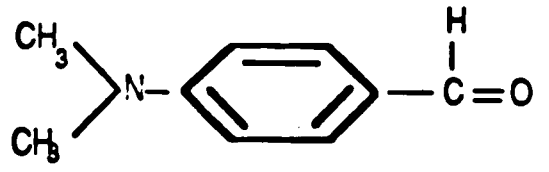

DABA(CH-O)

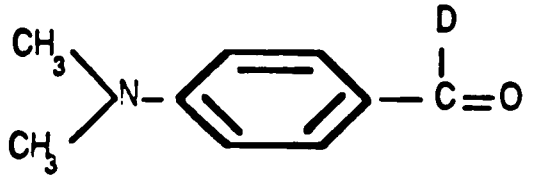

DABA(CD-O)

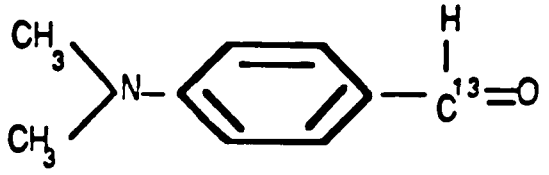

DABA(C^{13})

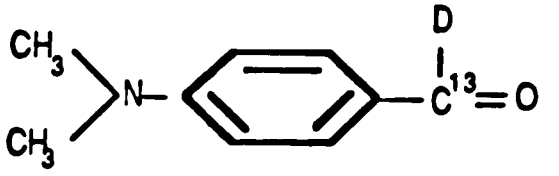

DABA(C^{13}+D)

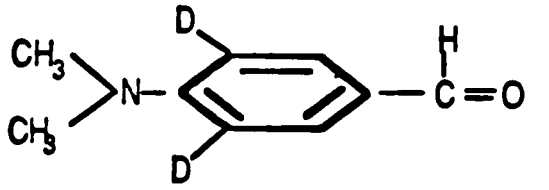

DABA(2D)

Figure 13.

Figure 14: Raman spectra of: (a) 4.6 mM DABA in 0.1 M pyrophosphate buffer pH 9.6; (b) DABA bound to LADH; (c) DABA-Zn complex in methylene chloride. All conditions are the same as those in Figure 4.

(a) DABA(CHO) in pH 9.6 buffer
359
596
633
729
840
944
1000
1178
1253
1403
1419
1443
1548
1592
1644
(b) DABA(CHO) bound to LADH
367
605
635
734
848
944
1180
1228
1321
1353
1378
1393
1443
1545
1578
1624
(c) Zn-DABA(CHO) in CH_2Cl_2
382
500
610
637
842
941
995
1177
1228
1269
1326
1354
1378
1398
1443
1545
1582
1626
300
400
500
600
700
800
900
1000
1100
1200
1300
1400
1500
1600
1700
Δ Wave Number (cm^{-1})

Figure 14.

site of LADH, when the substrate DABA binds. Therefore, as a first working assumption one could surmise that the DABA is directly complexed with the zinc ion in situ.

The juxtaposition of spectra in Figure 14 with those of Figure 15 presents several implications. It is apparent that the 1403 cm^{-1} band in the DABA spectrum in Figure 15a arises from the aldehydic C-H bending mode of DABA. This mode seems to shift when DABA is deuterated (Figure 15b). From theoretical calcultaions it is known that a pure hydrogen bending mode at~1400 cm^{-1} would decrease by ~$\sqrt{2}$ or 990 cm^{-1}. From Figure 15 one may observe a shift to 1044 cm^{-1}, closely resembling the value obtained theoretically for C-H bending modes.

The 1378 cm^{-1} band in Figure 14 is likely to contain a substantial contribution from C-O-Zn^{++} (Figure 16). This band is not observed in the Raman spectrum of the native DABA but appears in the Raman spectrum of the DABA in complexation to the zinc ion and in situ. Additionally, the deuteration of the aldehydic proton (Figure 16) seems to cause a downward shift in the band about 100 cm^{-1} to 1289 cm^{-1} when the DABA is in complexation with the zinc ion or at the active site of the enzyme (Figure 17). Moreover, when contrasting ^{12}CDO to ^{13}CDO (Figure 17) the mode shifts further downward by about 6 cm^{-1}.

The ring structure of DABA it seems contributes substantially to its Raman spectrum. This observation is based on the various peak shifts which occurs when the ring is deuterated (Figure 15).

Figure 15: Raman spectra of: (a) 4.6 mM DABA; (b) 7.3 mM DABA(CDO); (c) 2.2 mM DABA(^{13}CDO); (d) 4.3 mM DABA(^{13}CHO); (e) 2.5 mM DABA(2D). All conditions are the same as those in Figure 4.

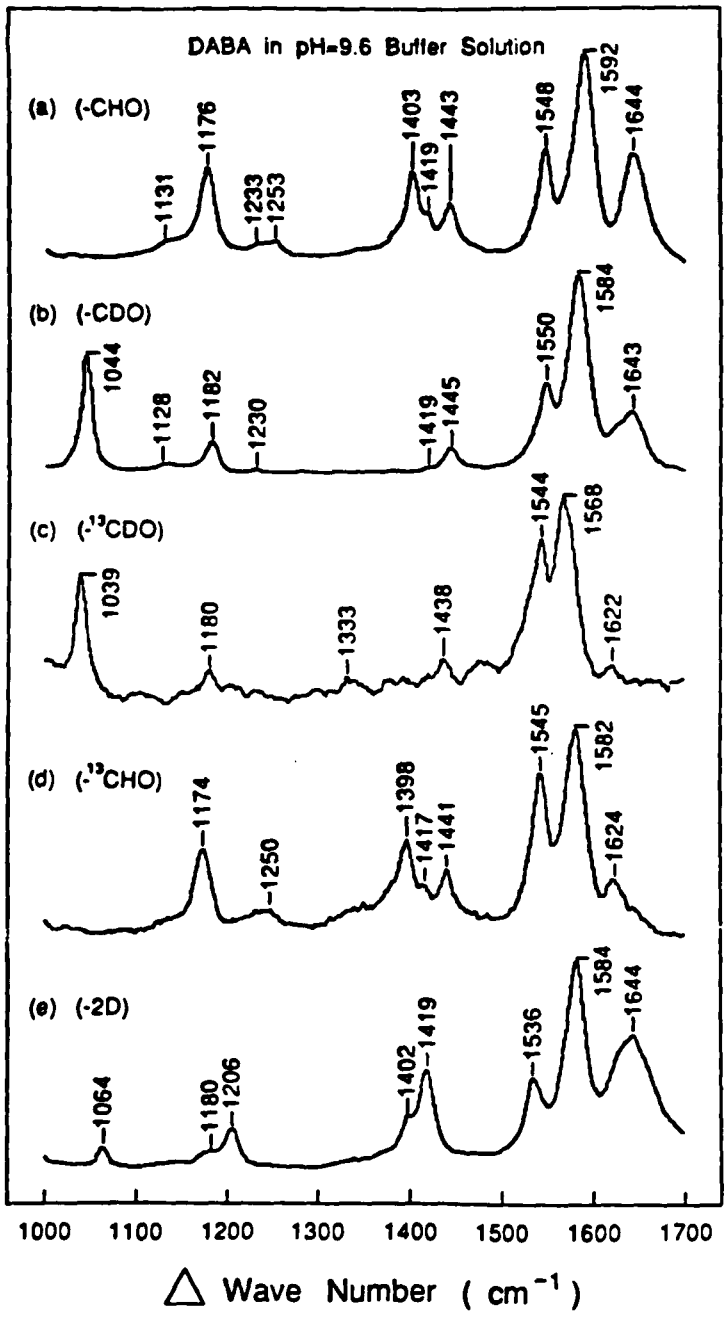
DABA in pH=9.6 Buffer Solution
(a) (-CHO)
1131
1176
1233
1253
1403
1419
1443
1548
1592
1644
(b) (-CDO)
1044
1128
1182
1230
1419
1445
1550
1584
1643
(c) (-^{13}CDO)
1039
1180
1333
1438
1544
1568
1622
(d) (-^{13}CHO)
1174
1250
1398
1417
1441
1545
1582
1624
(e) (-2D)
1064
1180
1206
1402
1419
1536
1584
1644
1000
1100
1200
1300
1400
1500
1600
1700
Wave Number (cm^{-1})

Figure 15.

Figure 16: Raman spectra of DABA zinc complexes (a) 20 mM DABA; (b) 28 mM DABA(CDO); (c) 40 mM DABA(^{13}CDO); (d) 20 mM DABA(^{13}CHO); (e) 19 mM DABA(2D). All samples were in methylene chloride. All conditions are the same as those in Figure 4.

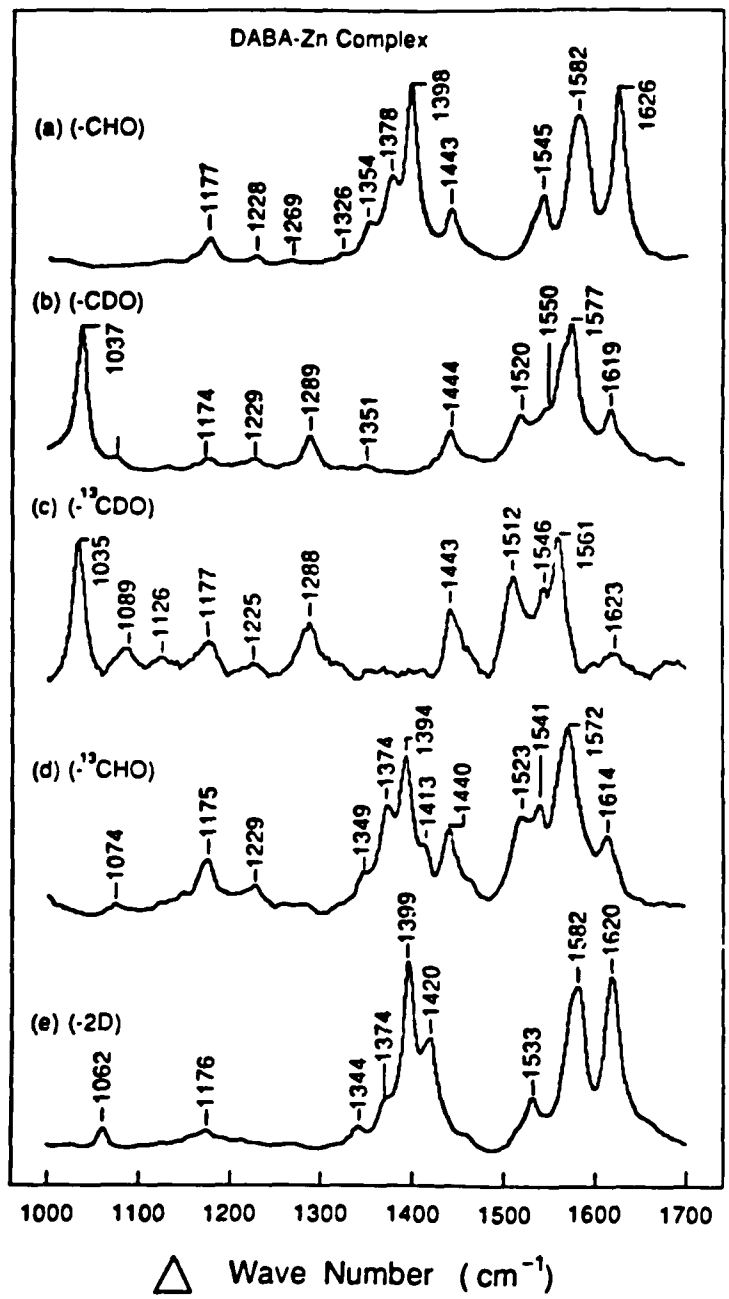
DABA-Zn Complex
(a) (-CHO)
1177
1228
1269
1326
1354
1378
1398
1443
1545
1582
1626
(b) (-CDO)
1037
1174
1229
1289
1351
1444
1520
1550
1577
1619
(c) (-13CDO)
1035
1089
1126
1177
1225
1288
1443
1512
1546
1561
1623
(d) (-13CHO)
1074
1175
1229
1349
1374
1394
1413
1440
1523
1541
1572
1614
(e) (-2D)
1062
1176
1344
1374
1399
1420
1533
1582
1620
1000
1100
1200
1300
1400
1500
1600
1700
Δ Wave Number (cm-1)

Figure 16.

Figure 17: Raman spectra of DABA bound to LADH: (a) DABA; (b) DABA(C DD); (c) DABA(^{13}CDO); (d) DABA (^{13}CHO); (e) DABA(2D). The molar concentration in all cases is 0.67 mM. All other conditions are the same as those in Figure 4.

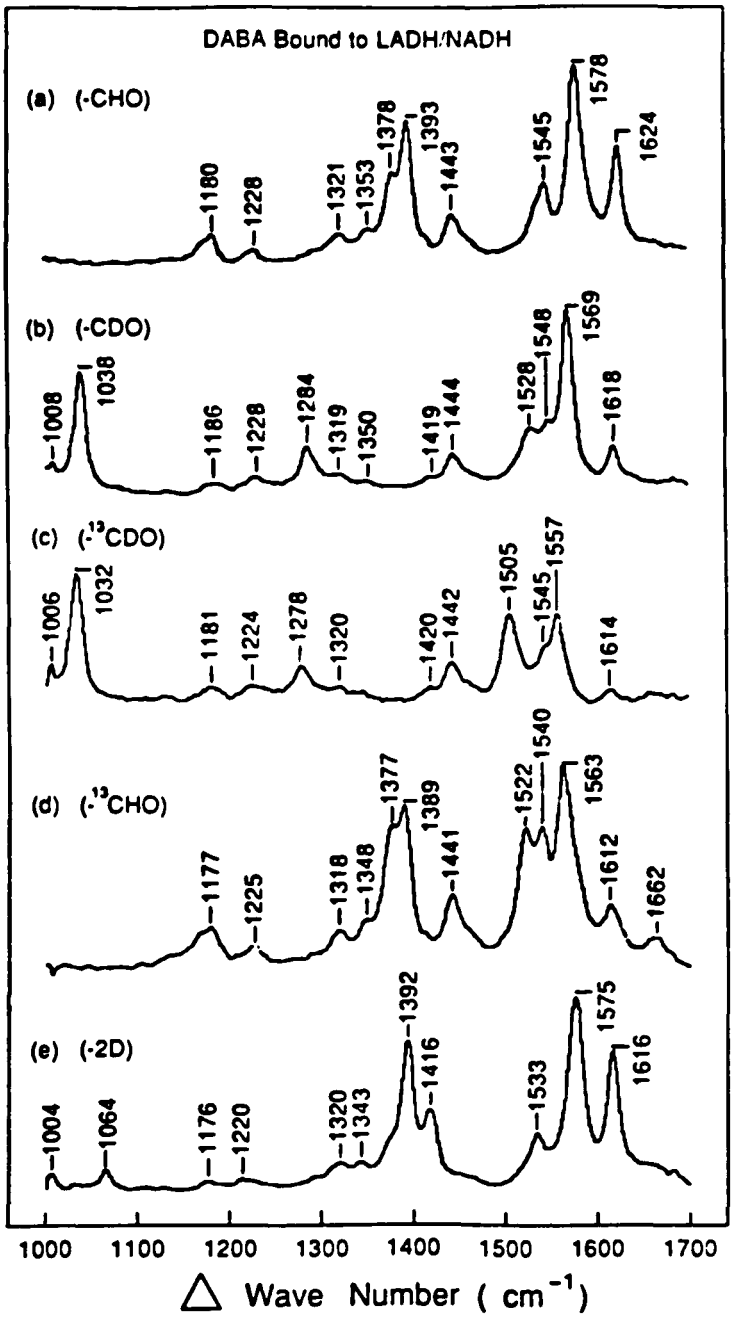
DABA Bound to LADH/NADH
(a) (-CHO)
1180
1228
1321
1353
1378
1393
1443
1545
1578
1624
(b) (-CDO)
1008
1038
1186
1228
1284
1319
1350
1419
1444
1528
1548
1569
1618
(c) (-13CDO)
1006
1032
1181
1224
1278
1320
1420
1442
1505
1545
1557
1614
(d) (-13CHO)
1177
1225
1318
1348
1377
1389
1441
1522
1540
1563
1612
1662
(e) (-2D)
1004
1064
1176
1220
1320
1343
1392
1416
1533
1575
1616
1000
1100
1200
1300
1400
1500
1600
1700
Wave Number (cm-1)

Figure 17.

It seems likely from these studies that the DABA-Zn^{++} complex in methylene chloride is a possible model for aromatic aldehydes at the active site of the enzyme liver alcohol dehydrogenase. This observation is based on the striking resemblance of the resonance Raman spectra of the aromatic aldehyde DABA and its isotopically labelled derivatives, when at the zinc (II)-containing active site of LADH, as compared to those of DABA and its isotopic derivatives in complexation with zinc ion in methylene chloride. Further evidence for the support of this model comes from the striking resemblence of the Raman spectrum of the DABA-Zn complex and the spectrum of DABA in situ at lower wavenumbers. For example the relative intensities of the bands in the 590-640 cm^{-1} region of these spectra (Figure 14) are the same. It is worth noting that the lower wavelength peak height in this region is small relative to the higher wavelength peak, for both the in situ data and the zinc (II) complex data. However, in the DABA solution spectrum the relative intensities of these peaks has the opposite appearance with the lower wavelength peak being higher than the higher wavelength peak.

B) Analysis of the DABA spectrum

In relative terms the DABA molecule is a rather simple molecule. It is clear from our data that, although DABA shows a substantial Raman spectrum, its Raman spectrum poses some difficulty in interpreting. It seems obvious, therefore that one

must exercise caution in assigning any of these peaks to particular bending or stretching modes in the molecule. However, in looking at the data systematically we find that the bands in the region of 1000-1700 cm^{-1} are greatly affected when the aldehydic proton is deuterated (compare Figure. 15a with Figure. 15b). These affects have also been observed for the other isotopic derivatives of DABA.

In viewing the Raman spectrum of DABA from the higher wavenumber frequencies to those of the lower wavenumber frequencies, we have consistently observed a peak at 1700 cm^{-1} (data not shown) in spectra of DABA bound to the active site of LADH and when in complexation with zinc ion in methylene chloride. At this time it is quite difficult to access the origin of this peak. However, we have observed that the relative intensities, of the two highest wavenumber peaks of the various DABA spectra, are a function of the excitation wavelength. When the excitation wavelength becomes longer the intensity of the highest frequency peak decreases while that of the lowest frequency peak increases.

Considering more specific portions of this 1000-1700 cm^{-1} region of the DABA spectra, it is tempting to assign the 1500-1700 cm^{-1} region as being due to the carbonyl stretch, for it is usually in this region that carbonly stretching frequencies are found. Upon close examination of the 1644 cm^{-1} mode for DABA in solution it seems that this mode contains more than one peak (Figure. 14). The juxaposition of this peak with the 1625 cm^{-1} band found in the Raman spectrum of the zinc ion complex and <u>in situ</u> suggest that

one of the peaks which composes the 1644 cm^{-1} peak in the solution spectrum "disappears" in forming the Zn-oxygen bond, since it becomes narrower. This peak tends to be downshifted slightly with a reduction in intensity in most of the Raman spectra of the isotopic derivatives of DABA.

In turn we look at the DABA bound to the LADH/NADH binary complex. Upon substituting the carbonyl carbon with ^{13}C, (Figure. 17d), it seems likely that the carbonyl stretch is coupled to all of the modes in this region for all of the peaks in this area are affected by this substitution (compare Figure. 17a to Figure. 17d). For example the 1578 cm^{-1} peak is shifted by 15 wave numbers to 1563 cm^{-1}. It is known that for a "pure" carbonly stretch a shift of ~35 cm^{-1} is expected. In addition, upon deuteration of the aldehydic proton of the ^{13}C derivative (Figure. 17c) this peak shifts to 1557 cm^{-1}. It is worth noting that deuteration of the carbons at the 3 and 5 positions of the ring has little or no affects on this band, (Figure. 17e).

In terms of the DABA-Zn^{++} complex it is quite apparent that this spectral band contains more than one peak at ~1582 cm^{-1} (Figure. 16a). When the aldehydic proton is deuterated the 1578 cm^{-1} peak becomes more pronounced with a shoulder on its lower frequency side (Figure. 16b). In addition this peak becomes somewhat assymmetric upon ^{13}C labelling of the carbonyl carbon (Figure. 16d). There is a peak at 1545 cm^{-1} which is assymetric in the LADH/NADH/DABA(CHO) (Figure. 17a) spectrum. Isotopic labelling

of DABA seems to have some affects on this band. For example there is a pronounced separation of two bands which apparently arises from this band. With ^{13}C label of the functional group the relative intensity of the peak at the lower wavenumber frequency is heightened. It is not clear whether deuteration of C3 and C5 of the ring has any affects on this mode.

The region from 1250-1500 cm^{-1} has some outstanding features. The peak at 1444 cm^{-1} is strongly affected by deuteration of the C3 and C5 carbons of the ring. It "disappears" in all 2D spectra with the evolution of a new peak at 1416 cm^{-1} in the LADH/NADH/DABA spectrum (Figure. 17). It seems clear, therefore, that this mode can be assigned to the bending motions of the ring's hydrogen atoms. Upon analysing the Raman spectrum of bound DABA and DABA-Zn^{++} complex, in this region and comparing them to the solution spectrum of DABA, it seems likely that one of the two peaks around 1390 cm^{-1} in the LADH/NADH/DABA and zinc (II)-DABA spectra may be due to the weakened carbonyl stretch which results from the Zn-oxygen bond. However, ^{13}C substitution suggests that this is not the case, since it has little or no affects on these modes (Fig. 16d and 17d). On the other hand, the spectrum of the deuterated aldehydic proton shows no peaks in this location (Figure. 16b and Figure. 17b), while exhibiting two new peaks at 1284 cm^{-1} and 1038 cm^{-1}. In addition a comparable downshift of the 1403 cm^{-1} to 1044 cm^{-1} was observed in the solution spectrum of DABA as well. As mentioned above "pure" hydrogen bending modes

around 1400 cm^{-1}, theoretically, should be shifted $\sim\sqrt{2}$ or 990 cm^{-1} upon deuteration. This value is obtained from a simple reduced mass calculation on an isolated hydrogen bending mode, when the hydrogen is replaced by a deuterium. Therefore, it seems likely that these modes around 1400 cm^{-1} in both bound and free DABA spectra are mostly due to the aldehydic proton bending mode. Although some contribution to these peaks are clearly from the ring hydrogen, since substitution on the ring results in the reduction in intensity of these peaks. Tentatively, in our laboratory, we have assigned the 1403 cm^{-1} mode to coupled hydrogen bending in both the functional group and the ring structure of DABA.

We make mention of the peaks at 1353 cm^{-1}, 1321 cm^{-1}, 1228 cm^{-1} and 1180 cm^{-1} in the LADH/NADH/DABA and zinc ion complex spectra. We have noticed that these peaks go unchanged in the spectra of the isotopic derivatives of DABA. This implies that these peaks might be the results of the ring skeleton stretching. Further evidence for this conditional assignment lies with the fact that they are slightly different in the solution spectrum as compared to the bound or zinc (II) complex spectrum. It is important to point out that these modes are seriously affected in the solution spectrum of 2D.

Figures 18 and 19 show the Raman spectra of the low frequency range of DABA and its isotopically labelled derivatives in pyrophosphate buffer, pH 9.6, and when bound to the enzyme,

Figure 18: Low frequency range of DABA spectra found in Figure 15.

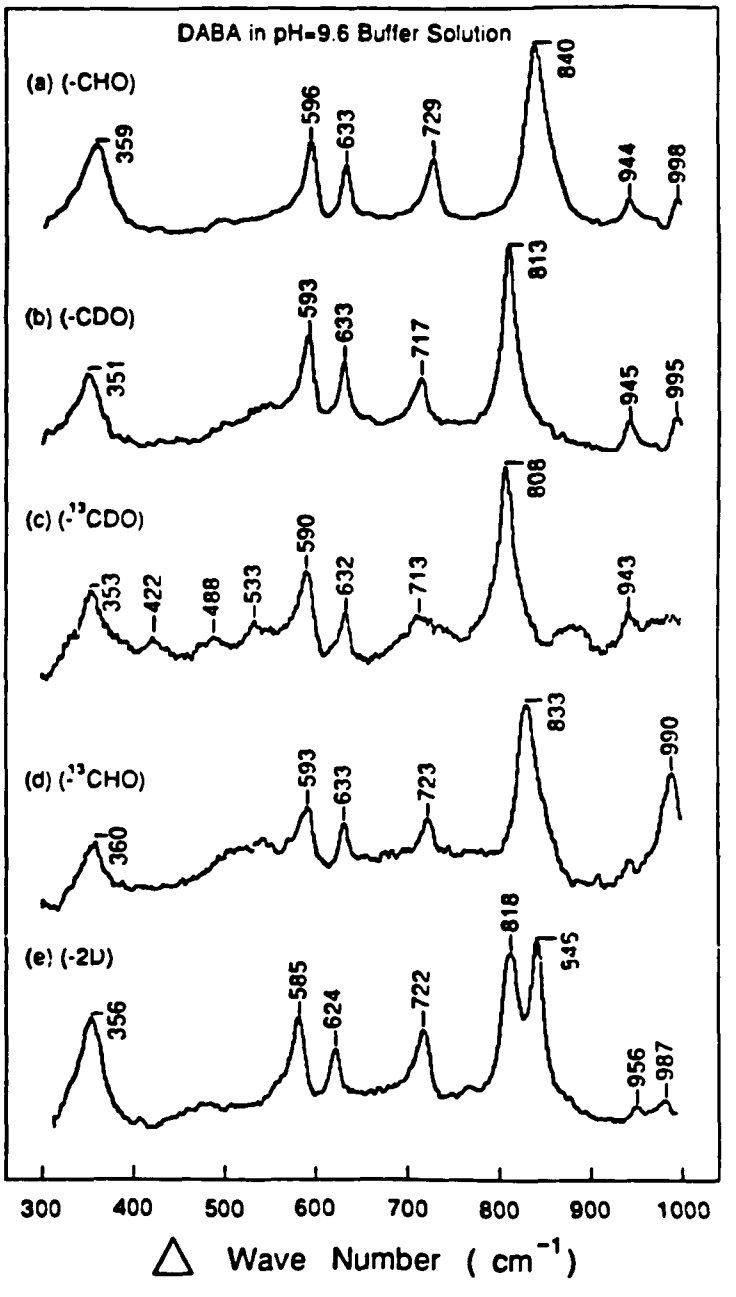
DABA in pH=9.6 Buffer Solution
(a) (-CHO)
359
596
633
729
840
944
998
(b) (-CDO)
351
593
633
717
813
945
995
(c) (-13CDO)
353
422
488
533
590
632
713
808
943
(d) (-13CHO)
360
593
633
723
833
990
(e) (-2D)
356
585
624
722
818
545
956
987
300
400
500
600
700
800
900
1000
Wave Number (cm-1)

Figure 18.

Figure 19: Low frequency range of DABA spectra found in Figure 17.

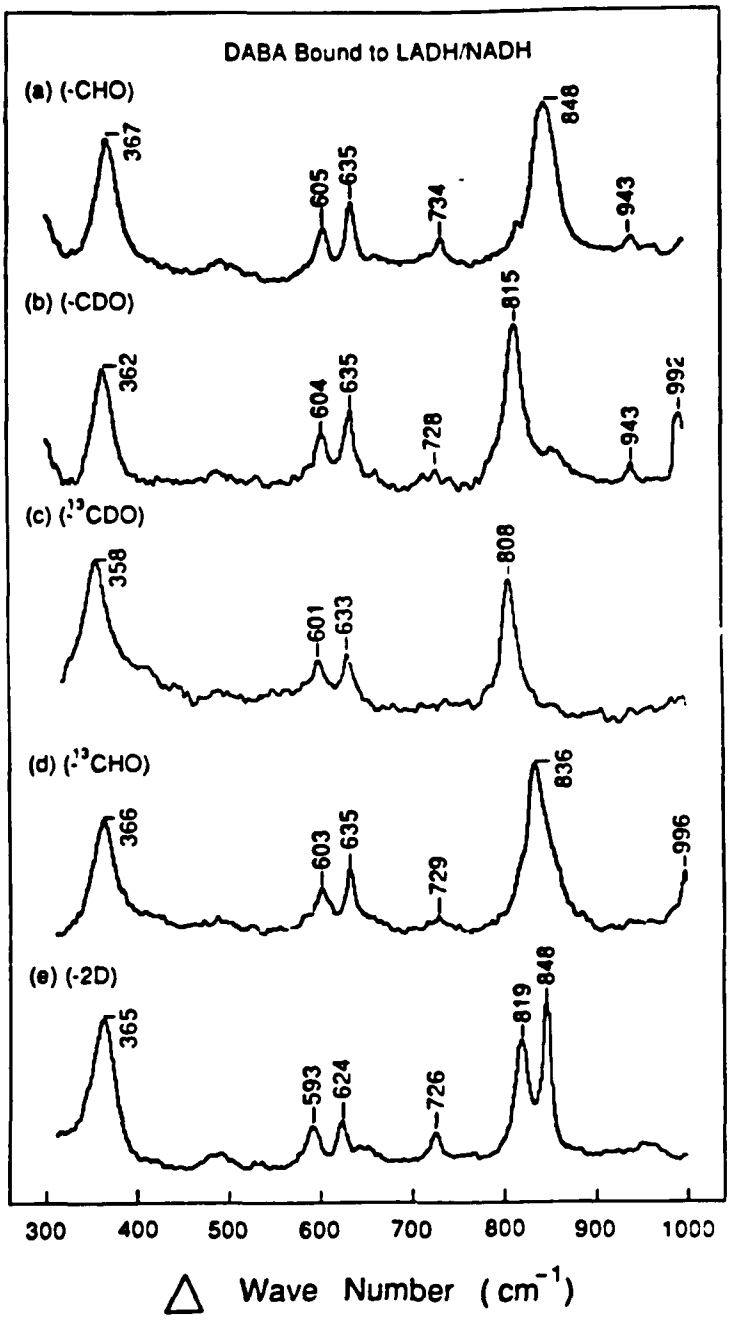
DABA Bound to LADH/NADH
(a) (-CHO)
367
605
635
734
848
943
(b) (-CDO)
362
604
635
728
815
943
992
(c) (-^{13}CDO)
358
601
633
808
(d) (-^{13}CHO)
366
603
635
729
836
996
(e) (-2D)
365
593
624
726
819
848
300
400
500
600
700
800
900
1000
Δ Wave Number (cm^{-1})

Figure 19.

LADH, respectively. The peak at 848 cm^{-1} (Figures. 14b and 19a) is very broad, in these spectra as well as in the $zinc^{++}$-DABA complex Raman spectrum (data not shown). In the spectrum for DABA, deuterated in the ring at C3 and C5, this peak splits into two peaks (Figure. 19e). It is also affected by the isotopic labels of the aldehydic functinal group (Figure. 18b,c,d and Figure. 19b,c,d), as it shows a profound downshift, under these conditions.

It is worth remembering that the relative intensity pattern for the 635 cm^{-1} and 605 cm^{-1} in the in situ spectrum jibes quite well with the zinc ion complex Raman spectrum and that these modes show just the opposite relative intensities in the DABA solution spectrum. Beside this fact, these peaks seem to be insensitive to isotopic substitution of the aldehydic carbon and proton atoms, but show significant downshift when the C3 and C5 carbons of the ring are deuterated. This insensitivity to isotopic substitution is observed for these peaks in the solution spectrum as well. The broad peak at 367 cm^{-1} under all conditions of DABA (i.e. bound, complexed to zinc (II) or in solution), show insensitivity to any isotopic substitution. Furthermore the position of this peak in the DABA spectrum when bound to LADH/NADH, 367 cm^{-1}, closely resembles the solution data, 359 cm^{-1}, than it does the zinc ion complex data, 382 cm^{-1}. To date, accessing the behavior of these peaks poses some difficulties.

SUMMARY

Equine liver alcohol dehydrogenase (EC-1.1.1.1.), LADH, catalyzes the oxidation of various primary and secondary alcohols to the corresponding aldehydes (14,90) along with the reduction of the coenzyme nicotinamide adenine dinucleotide, NAD^+. Eklund et al. (35) reported a detailed three-dimensional structure at 2.4 Å resolution with X-ray diffraction of crystalline LADH. Additional results have been obtained with X-ray diffraction and solution spectroscopy of LADH complexed with coenzyme or its various analogues and its ternary complexes with different substrates or inhibitors (1,36,74). The recent work of Abdallah et al. (2) provides an elegant example of such a study.

In our laboratory we have examined the solution Raman spectrum of LADH. Based on the method of William et al. (101), whose calculation of structure rests upon the amide I bands, we found that LADH in solution contains 21% α helices, 35% β-pleated sheets, and 43% random coil. These values coincide, to a large extent with those obtained from X-ray crystallography (29% α helices, 34% β-pleated sheets and 37% random coil). These differences in structure from solution to crystalline state may reflect minute conformational changes which may occur upon dissolving the crystals in solution.

Currently, a wealth of information has accumulated on how coenzymes and substrates bind to dehydrogenases in an attempt at

understanding mechanistically how these enzymes catalyze the conversion of substrates into products. It is well known that oxidized nicotinamide adenine dinucleotide (NAD^+) and its reduced form (NADH) are coenzymes for hundreds of enzymatic oxidation-reduction reactions (31). However, the nature of the interaction of these cofactors with proteins is not understood. Some information on this interaction is available from X-ray crystallographic studies on several dehydrogenases (14,37,42,44,69,74,77). In these studies, electron-density differences were calculated to give the location of the ligand within the protein. Nevertheless, the nature of the interaction(s) between the ligand and protein can only be deduced and not studied directly with this technique.

In turn we have employed Raman spectroscopy which gives valuable information on normal mode vibrations of atoms within a molecule, for it is sensitive to bonding changes which may accompany ligand binding to proteins. Using difference Raman techniques the spectrum of NADH bound to LADH was attained. Several obvious changes can be seen when NADH binds to LADH as compared to that in solution. These spectral changes suggest that the nicotinamide and the adenine moieties of NADH are directly involved when NADH binds LADH. This is indicated by the disappearance of the 1545 cm^{-1} band, associated with the nicotinamide moiety and the 1338 cm^{-1} band, due to the adenine moiety, in the spectrum when the coenzyme binds NADH relative to

NADH's solution spectrum. The absence of the 1545 cm^{-1} peak in the LADH/NADH complex connotes the involvement of one of the NH_2 groups in binding, since the 1545 cm^{-1} mode is sensitive to the carboxamide.

Particulars of the Raman spectral features of NADH and NAD^+ have been investigated by studying analogues and fragments of the molecules as a means of understanding the spectroscopy of free and bound coenzyme. The effects of deuteration of the exchangeable protons and of pH on the Raman spectra were studied as well. It is well known that these coenzymes are composed of nicotinamide in the form of a quaternary ammonium salt, two molecules of D-ribose linked as pyrophosphate esters and the heterocyclic component adenine (Figure. 10). It is also known that these coenzymes at room temperature in solution exist in closed forms, i.e. the nicotinamide moiety and the adenine moiety are stacked together (27,60). However, we have observed no significant changes, except for a slight downward shift of the 1545 cm^{-1} band, in the Raman spectra of either NADH of NAD^+ when subjected to 8M urea, a strong destacking agent, or in the case of NADH, 75°C (NAD^+ is unstable at high temperatures). As a result we have assigned the Raman peaks of NADH and NAD^+ to smaller moieties of these molecules. We have also noticed major changes in the Raman spectrum associated with the adenine moeity when adenine is protonated at pH 3.9.

The binding nature of the aromatic aldehyde, DABA, to the catalytic Zn^{++} active site of LADH has been studied using pre-resonance Raman spectroscopy and has been compared to the $zinc^{++}$-DABA complex. We have isotopically labelled the functional group of the compound with ^{13}C and deuterium in various combinations and have deuterated the C3 and C5 positions of the ring in order to understand the normal mode patterns of DABA, when bound to the enzyme and in solution. We find a striking correspondence between the Raman spectra of bound DABA and the DABA-Zn^{++} complexes. This resemblance extends to all of the isotopic derivatives studied.

In an attempt at interpreting the Raman spectrum of DABA we find that the observed Raman bands arise from highly delocalized normal modes in most cases. The bands in the 1500-1700 cm^{-1} region contain C=C and C=O stretch with some C-H and C-C-C bending contribution. There are marked changes in the bands when DABA binds LADH/NADH. Bands in the 1250-1500 cm^{-1} region are due mainly to C-H bending motions with some stretching characteristics. There are no obvious changes in these modes when DABA binds LADH/NADH. In viewing the lower portion of the spectrum i.e. below ~1200 cm^{-1} it seems difficult in assessing the behavior of these modes as of now.

Our data suggest that the carbonyl retains a significant portion of its double bond characteristic when DABA binds LADH. However, this double bond feature is substantially less than that

found in the solution spectrum of DABA. This observation is based on the response to ^{13}C labelling, of those bands found in the 1500-1700 cm^{-1} region.

The ring structure contributes substantially to the Raman spectrum of DABA. This observation is supported by the numerous peak shifts which occurs when the ring is deuterated (Figure. 19).

REFERENCES

1. Abdallah, M. A., Biellmann, J.-F., Nordström, B., & Brändèn, C.-I. (1975) Eur. J. Biochem. 50, 475-481.

2. Abdallah, M., Biellmann, J.-F., Cedergren-Zeppezauer, R., Gerber, M., Dietrich, H., Zeppezauer, M., Koerber, S., MacGibbon, A., & Dunn, M. (1984) Biochemistry 23, 1003-1015.

3. Adams, M. J., Buehner, M., Chandrasekhar, K., Ford, G. C., Hackert, M. L., Liljas, A., Rossman, M. G., Smiley, I. E., Allison, W. S., Everse, J., Kaplan, N. O., & Taylor, S. S. (1973) Proc. Natl. Acad. Sci. U.S.A. 70, 1968-1972.

4. Alberty, R. A., Smith, R. M., & Bock, R. M. (1951) J. Biol. Chem. 193, 425-434.

5. Alnon, D. I. (1952) Science 116, 635-639.

6. Angelis, C. T., Dunn, M. F., Muchmore, D. C., Wing. R. M. (1977) Biochemistry 16, 2922-2931.

7. Banaszak, L. J., & Bradshaw, R. A. (1975) in The Enzymes, Vol. XI, 3rd ed., (Boyer, P. D., Ed.) pp 369-396, Academic Press, New York.

8. Barrett, T. W. (1980) J. Raman Spectros. 9, 130-133.

9. Biellmann, J.-F., & Jung, M. J. (1971) Eur. J. Biochem. 19, 130-134.

10. Blout, E. R., DeLoaè, C., & Asadourian, A. (1961) J. Am. Chem. Soc. 83, 1895-1900.

11. Bock, R. M., Ling, N.-S., Morell, S. A., & Lipton, S. H. (1956) Arch. Biochem. Biophys. 62, 253-264.

12. Bowman, W. D., & Spiro, T. G. (1980) J. Raman Spectros. 9, 369-371.

13. Brändèn, C.-I. (1965) Arch. Biochem. Biophy. 112, 215-217.

14. Brändèn, C.-I., Jörnvall, H., Eklund, H., & Furugren, B. (1975) in The Enzymes, Vol. XI, 3rd ed., (Boyer, P. D., Ed.) pp 103-190, Academic Press, New York.

15. Broomhead, J. M. (1951) Acta Crystallogr. 4, 92-100.

16. Bushaw, T. H., Lytle, F. E., & Tobias, R. S. (1980) Appl. Spectrosc. 34, 521-525.

17. Callender, R. H. & Honig, B. (1977) Ann. Rev. Biophys. Bioeng. 6, 33-55.

18. Carey, P. R. (1978) Q. Rev. Biophys. 11, 309-370.

19. Carey, P. R. & Salares, V. R. (1980) Adv. Infrared Raman Spectrosc. 7, 1-55.

20. Carey, P. R. & Storer, A. C. (1984) Ann. Rev. Biophys. Bioeng. 13, 25-49.

21. Catterall, W. A., Hollis, D. P., & Walter, C. F. (1969) Biochemistry 8, 4032-4036.

22. Chen, M. C. & Lord, R. C. (1974), J. Am. Chem. Soc. 96, 4750-4752.

23. Chen, D., Yue, K. T., Martin, C., Rhee, K. W., Sloan, D. L., and Callender, R. (1987) Biochemistry 26 (in press).

24. Chinsky, L. Turpin, P. Y., Duquesne, M., & Brahms, J. (1978) Biopolymers 17, 1347-1359.

25. Cochran, W. (1951) Acta Crystallogr. 4, 82-92.

26. Cook, P. F., Oppenheimer, N. J., Cleland, W. W. (1981) Biochemistry 20, 1817-1825.

27. Cross, D. G., & Fisher, H. F. (1969) Biochemistry 8, 1147-1155.

28. Dalziel, K. (1957) Acta Chem. Scand. 11, 397-398.

29. Dalziel, K. (1961) Biochem. J. 80, 440-445.

30. Dalziel, K. (1963) J. Biol. Chem. 238, 2850-2858.

31. Dalziel, K. (1975) in The Enzymes, Vol. XI, 3rd ed., (Boyer, P. D.,Ed.) pp 1-60, Academic Press, New York.

32. DeTraglia, M. C., Schmidt, J., Dunn, M. F., & McFarland, J. T. (1977) J. Biol. Chem. 252, 3493-3500.

33. Drum, D. E., Harrison, I. H., IV, Li, T.-K., Bethune, J. L., and Vallee, B. L. (1967) Proc. Natl. Acad. Sci. USA 57, 1434-1440.

34. Drum, D. E., Li, T.-K., and Vallee, B. L. (1969) Biochemistry 8, 3792-3797.

35. Eklund, H., Nordström, B., Zeppezauer, E., Söderlund, G., Ohlsson, I., Boiwe, T., Söderberg, B.-O., Tapia, O., & Brändèn, C.-I. (1976) J. Mol. Biol. 102, 27-59.

36. Eklund, H. & Brändèn, C.-I. (1979) J. Biol. Chem. 254, 3458-3461.

37. Eklund, H., Samama, J.-P., Wallèn, L., Brändèn, C.-I., Åkeson, Å., & Jones, T. A. (1981) J. Mol. Biol. 146, 561-587.

38. Ellis, P. D., Fisher, R. R., Dunlap, R. B., Zens, A. P., Bryson, T. A., & Williams, T. J. (1973) J. Biol. Chem. 248, 7677-7681.

39. Felton, R. H. & Yu, N.-T. (1978) in The Porphyrins, Vol. III, part A, (Dolphin, D., ed) pp 347-393, Academic Press, New York.

40. Fodor, S. P. A., & Spiro, T. G. (1985) Biophys. J. 47, 502a.

41. Forrest, G. (1976) J. Phys. Chem. 80, 1127-1128.

42. Harris, I. I., & Waters, M. (1976) in The Enzymes, Vol. XIII, 3rd ed., (Boyer, P. D., Ed.) pp 1-49 Academic Press, New York.

43. Hollis, D. P. (1967) Biochemistry 7, 2080-2087.

44. Holbrook, J. J., Liljas, A., Steindel, S. J., & Rossmann, M. G. (1975) in The Enzymes, Vol. XI, 3rd ed., (Boyer, P. D., Ed.) pp 191-292, Academic Press, New York.

45. Iweibo, K. & Weiner, H. (1972) Biochemistry 11, 1003-1010.

46. Jagodzinski, P. W. & Peticolas, W. L. (1981) J. A. C. S. 103, 234-236.

47. Jagodzinski, P. W., Funk, G. F. & Peticolas, W. L. (1982) Biochemistry 21, 2193-2202.

48. Jardetzky, C. D., & Jardetzky, O. (1960) J. Am. Chem. Soc. 82, 222-229.

49. Kint, S., & Tomimatsu, Y. (1979) Biopolymers 18, 1073-1079.

50. Kubasek, W. L., Hudson, B., & Peticolas, W. L. (1985) Proc. Natl. Acad. Sci. USA 82, 2369-2373.

51. Lafleur, L., Rice, J., & Thomas, Jr., G. J. (1972) Biopolymers 11, 2423-2437.

52. Lippert, J. L., Tyminski, D., & Desmeules, P. (1976) J. Am. Chem. Soc. 98, 7075-7080.

53. Lord, R. C., & Thomas, Jr., G. J. (1967) Spectrochim. Acta 23A, 2551-2591.

54. Lord, R. C. & Yu, N. T. (1970) J. Mol. Biol. 50, 509-524.

55. Luisi, P. L., & Favilla, R. (1970) Eur. J. Biochem. 17, 91-94.

56. Maret, W., Anderson, I., Dietrich, H., Schneider-Bernlohr, H., Einarsson, R., & Zeppezauer, M. (1979) Eur. J. Biochem. 98, 501-512.

57. Maret, W., Zeppezauer, M., Sanders-Loehr, J., & Loehr, T. M. (1983) Biochemistry 22, 3202-3206.

58. Mathies, R. (1979) in Chemical and Biochemical Applications of Lasers, Vol. IV, (Moore, C. B., Ed.) pp 55, Academic Press, New York.

59. McDonald, G., Brown, B., Hollis, D., & Walter, C. (1972) Biochemistry 11, 1920-1930.

60. Meyer, W. L., Mahler, H. R., & Baker, Jr., R. H. (1962) Biochim. Biophys. Acta 64, 353-358.

61. Moore, C. E., Jr., & Underwood, A. L. (1969) Anal. Biochem. 29, 148-153.

62. Müller, D. (1933) Biochem. Z. 262, 239-.

63. Nason, A., Kaplan, N. O., & Colowick, S. (1951) J. Biol. Chem. 188, 397-406.

64. Nason, A., Kaplan, N. O., & Oldewurter, H. A. (1953) J. Biol. Chem. 201, 435-444.

65. Nishimura, Y., & Tsuboi, M. (1980) Science 210, 1358-1360.

66. Nishimura, Y., & Tsuboi, M. (1980b) Proc. Int. Conf. Raman Spectrosc., 7th, 568-571.

67. Nishimura, Y., Hirakawa, A. Y., & Tsuboi, M. (1978) Adv. Infrared Raman Spectrosc. 5, 217-275.

68. Nygaard, A. P., & Theorell, H. (1955) Acta Chem. Scand. 9, 1300-1305.

69. Ohlsson, I., Nordström, B., & Brändèn, C.-I. (1974) J. Mol. Biol. 89, 339-354.

70. Oppenheimer, N. J., Arnold, Jr., L. J., & Kaplan, N. O. (1978) Biochemistry 17, 2613-2619.

71. Oppenheimer, N. J. Arnold, L. J., Jr., & Kaplan, N. O. (1971) Proc. Natl. Acad. Sci. USA 68, 3200-3205.

72. Patrick II, D. M., Wilson, J. E., & Leroi, G. E. (1974) Biochemistry 13, 2813-2817.

73. Pezolet, M., Pigeon-Gosselin, M., & Coulombe, L. (1976) Biochim. Biophys. Acta 453, 502-512.

74. Plapp, B. V., Eklund, H., & Brändèn, C.-I. (1978) J. Mol. Biol. 122, 23-32.

75. Rimai, L., Cole, T., Parsons, J. L., Hickmott, J. T., Jr., & Carew, E. B. (1969) Biophys. J. 9, 320-329.

76. Rodgers, E. G., & Peticolas, W. L. (1980) J. Raman Spectros. 9, 372-375.

77. Rossmann, M. G., Liljas, A., Brändèn, C.-I., & Banaszak, L. J. (1975) in The Enzymes, Vol. XI, 3rd ed., (Boyer, P. D., Ed.) pp 61-102, Academic Press, New York.

78. Rothschild, K., Andrew, J., DeGrip, W. & Stanley, H. (1976) Science 191, 1176-1178.

79. Samama, J.-P., Zeppezauer, E., Biellmann, J.-F., & Brändèn, C.-I. (1977) Eur. J. Biochem. 81, 403-409.

80. Sarma, R. H., & Kaplan, N. O. (1970) Proc. Natl. Acad. Sci. U.S.A. 67, 1375-1382.

81. Schlessinger, J., Steinberg, I. Z., & Levitzki, A., (1975) J. Mol. Biol. 91, 523-528.

82. Shore, J. D., Weidig, C. F., Lodola, A., Parker, D. M., & Holbrook, J. J. (1975) Proc. of the Tenth FEBS Meet., 63-73.

83. Siamwiza, M. N., Lord, R. C., Chen, M. C., Takamatsu, T., Hanada, I., Matsura, H., & Shimanoychi, T. (1975) Biochemistry 14, 4870-4876.

84. Sloan, D. L., Young, J. M. & Mildvan, A. S. (1975) Biochemistry 14, 1998-2008.

85. Spiro, T. G. (1974) Acc. Chem. Res. 7, 339-344.

86. Subramanian, S., & Ross, P. D. (1977) Biochem. Biophys. Res. Comm. 78, 461-466.

87. Subramanian, S., & Ross, P. D. (1978) Biochemistry 17, 2193-2197.

88. Subramanian, S., Ross, J. B. A., Ross, P. D., & Brand, L. (1981) Biochemistry 20, 4086-4093.

89. Suhadolnik, R. J., Lennon, M. B., Uematsu, T., Monahan, J. E., & Baur, R. (1977) J. Biol. Chem. 252, 4125-4133.

90. Sund, H., & Theorell, H. (1963) in The Enzymes, Vol. VII, 2nd ed., (Boyer, P. D., Lardy, H., & Myrbäck, K., Ed.) pp 25-83, Academic Press, New York & London.

91. Theorell, H., & Chance, B. (1951) Acta Chem. Scand. 5, 1127-1144.

92. Theorell, H., & Tatemoto, K. (1971) Arch. Biochem. Biophys. 142, 69-82.

93. Thompson, S. T., Cass, K. H., & Stellwagen, E. (1975) Proc. Natl. Acad. Sci. USA 72, 669-672.

94. Tsuboi, M., Takahashi, S., & Harada, I. (1973) in Physico-Chemical Properties of Nucleic Acids (Duchesne, J., Ed.) Vol. 2, pp 91-145, Academic, London, New York.

95. Tsuboi, M. (1976) in Proceedings of the Fifth International Conference on Raman Spectroscopy, (Schmid, E. D., Ed.), Hans Ferdinand Schulz Verlag, Frieburg in Breisgan.

96. Vallee, B. L., Williams, R. J. P., & Hoch, F. L. (1959) J. Biol. Chem. 234, 2621-2626.

97. Wald, G., & Hubbard, R. (1950) Proc. Natl. Acad. Sci. USA 36, 92-102.

98. Warshel, A. (1977) Ann. Rev. Biophys. Bioeng. 6, 273-300.

99. Webb, L. E., Hill, E. J., & Banaszak, L. J. (1973) Biochemistry 12, 5101-5109.

100. Wierenga, R. K., DeMaeyer, M. C. H., & Hol, W. G. J. (1985) Biochemistry 24, 1346-1357.

101. Williams, R., Cutrera, T., Dunker, A. & Peticolas, W. (1980)

FEBS Lett. 115, 306-308.

102. Williams, R. Dunker, A., & Peticolas, W. (1980) Biophys. J. 32, 232-234.

103. Woenckhaus, C., Zoltobrocki, M., Berghäuser, J., & Jeck, R. (1973) Hoppe-Seyler's Z. Physiol. Chem. 354, 60-66.

104. Wolfe, J., Weidig, C., Halvorson, H., Shore, J., Parker, D., & Holbrook, J. (1977) J. Biol. Chem. 252, 433-436.

105. Wratten, C. C., & Cleland, W. W. (1963) Biochemistry 2, 935-941.

106. Young, J. M. & Wang, J. H. (1971) J. Biol. Chem 246, 2815-2821.

107. Yu, T. J. Lippert, J. L. & Peticolas, W. L., (1973) Biopolymers 12, 2161-2176.

108. Yu., N. T., Jo, B. H., Chang, R. C. C., & Huber, J. D. (1974) Arch. Biochem. 160, 614-622.

109. Yue, K. T., Yang, J.-P., Martin, C. L., Sloan, D. L., & Callender, R. H. (1984) Biochem. Biophys. Res. Comm. 122, 225-229.

110. Yue, K. T., Yang, J.-P., Martin, C. L., Lee, S. K., Sloan, D., L., & Callender, R. H. (1984) Biochemistry 23, 6480-6483.

111. Yue, K. T., Martin, C. L., Chen, D. H., Nelson, P., Sloan, D. L., & Callender, R. (1986) Biochemistry 25 4941-4947.

112. Zeppezauer, E., Söderberg, B.-O., Brändèn, C.-I., Åkeson, Å., & Theorell, H. (1967) Acta Chem. Scand. 21, 1099-1101.

113. Zubay, G. (1958) Biochim. Biophys. Acta 28, 644-645.